Article

Cell Chemical Biology

Quantitative Interactome Proteomics Reveals a Molecular Basis for ATF6-Dependent Regulation of a Destabilized Amyloidogenic Protein

Graphical Abstract

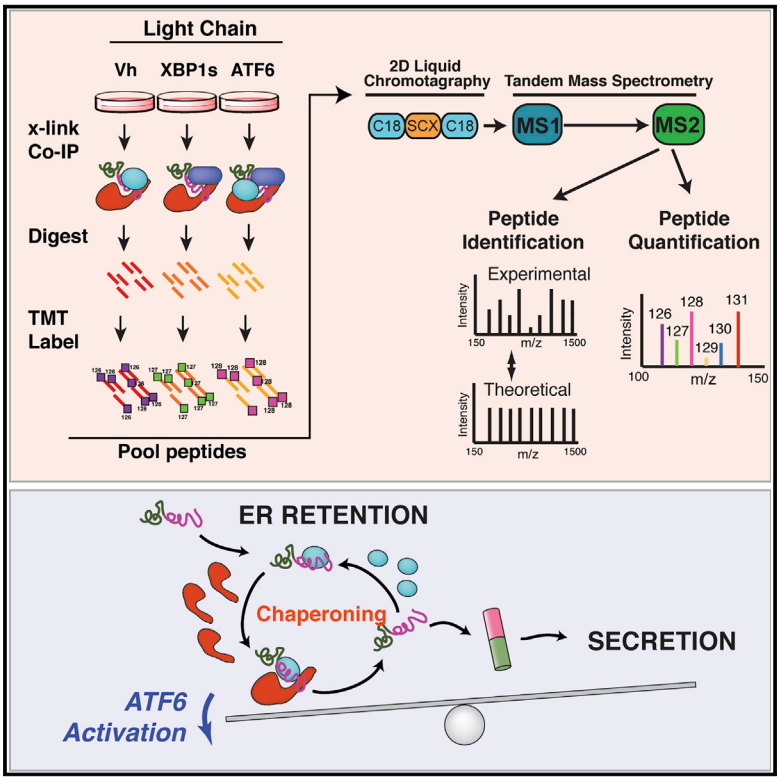

Highlights

- Quantitative proteomics defines the interactome for the amyloidogenic light chain ALLC
- ATF6 or XBP1s activation distinctly affect interactions between ALLC and ER proteins
- ATF6 activation reduces ALLC secretion through increased targeting to ER chaperones
- Enhanced quality control is based on global interaction changes coordinated by ATF6

Authors

Lars Plate, Bibiana Rius, Bianca Nguyen, Joseph C. Genereux, Jeffery W. Kelly, R. Luke Wiseman

Correspondence

wiseman@scripps.edu

In Brief

Activating the ATF6 arm of the unfolded protein response selectively reduces the secretion and subsequent toxic aggregation of destabilized amyloidogenic light chains. Plate et al. use a quantitative proteomics platform to identify specific ATF6-regulated ER proteostasis factors responsible for regulating the secretion of an amyloidogenic light chain from mammalian cells.

Plate et al., 2019, Cell Chemical Biology *26*, 1–13
July 18, 2019
https://doi.org/10.1016/j.chembiol.2019.04.001

CellPress

Please cite this article in press as: Plate et al., Quantitative Interactome Proteomics Reveals a Molecular Basis for ATF6-Dependent Regulation of a Destabilized Amyloidogenic Protein, Cell Chemical Biology (2019), https://doi.org/10.1016/j.chembiol.2019.04.001

Cell Chemical Biology
Article

Quantitative Interactome Proteomics Reveals a Molecular Basis for ATF6-Dependent Regulation of a Destabilized Amyloidogenic Protein

Lars Plate,[1,2,4,6] Bibiana Rius,[1,6] Bianca Nguyen,[1] Joseph C. Genereux,[1,2,5] Jeffery W. Kelly,[2,3] and R. Luke Wiseman[1,7,*]
[1]Department of Molecular Medicine, The Scripps Research Institute, 10550 North Torrey Pines Road, MB110, La Jolla, CA 92037, USA
[2]Department of Chemistry, The Scripps Research Institute, La Jolla, CA 92037, USA
[3]The Skaggs Institute for Chemical Biology, The Scripps Research Institute, La Jolla, CA 92037, USA
[4]Present address: Departments of Chemistry and Biological Sciences, Vanderbilt University, Nashville, TN, USA
[5]Present address: Department of Chemistry, University of California, Riverside, Riverside, CA, USA
[6]These authors contributed equally
[7]Lead Contact
*Correspondence: wiseman@scripps.edu
https://doi.org/10.1016/j.chembiol.2019.04.001

SUMMARY

Activation of the unfolded protein response (UPR)-associated transcription factor ATF6 has emerged as a promising strategy to reduce the secretion and subsequent toxic aggregation of destabilized, amyloidogenic proteins implicated in systemic amyloid diseases. However, the molecular mechanism by which ATF6 activation reduces the secretion of amyloidogenic proteins remains poorly defined. We employ a quantitative interactomics platform to define how ATF6 activation reduces secretion of a destabilized, amyloidogenic immunoglobulin light chain (LC) associated with light-chain amyloidosis (AL). Using this platform, we show that ATF6 activation increases the targeting of this destabilized LC to a subset of pro-folding ER proteostasis factors that retains the amyloidogenic LC within the ER, preventing its secretion. Our results define a molecular basis for the ATF6-dependent reduction in destabilized LC secretion and highlight the advantage for targeting this UPR-associated transcription factor to reduce secretion of destabilized, amyloidogenic proteins implicated in AL and related systemic amyloid diseases.

INTRODUCTION

The toxic extracellular aggregation of destabilized, amyloidogenic proteins is implicated in the onset and pathogenesis of diverse systemic amyloid diseases including light-chain amyloidosis (AL) and the transthyretin (TTR)-related amyloid diseases (Blancas-Mejia and Ramirez-Alvarado, 2013; Powers et al., 2009). A critical determinant in dictating the pathologic protein aggregation central to these diseases is the aberrant secretion of destabilized, aggregation-prone proteins to the extracellular space (Plate and Wiseman, 2017). The efficient secretion of these proteins increases their extracellular populations available for concentration-dependent aggregation into toxic oligomers and amyloid fibrils that deposit in distal tissues such as the heart, inducing organ dysfunction. The importance of amyloidogenic protein secretion in disease pathogenesis suggests that targeting the biological pathways responsible for regulating the secretion of destabilized, amyloidogenic proteins offers a unique opportunity to broadly ameliorate the pathologic extracellular protein aggregation implicated in the pathogenesis of diverse amyloid diseases (Plate and Wiseman, 2017).

Protein secretion through the secretory pathway is regulated by a process referred to as ER quality control (Balchin et al., 2016; Braakman and Bulleid, 2011; Feige and Buchner, 2014; Guerriero and Brodsky, 2012; Kim et al., 2013). In this process, newly synthesized proteins are co-translationally imported into the ER where they interact with ER chaperones and folding factors. These interactions facilitate the folding of proteins into their native conformations and prevent their misfolding and/or aggregation within the ER. Once folded, these proteins are packaged into vesicles for trafficking to downstream secretory environments including the extracellular space. Proteins unable to attain a native, folded conformation within the ER are instead recognized by ER degradation factors and directed toward degradation pathways such as ER-associated degradation (ERAD). Through this partitioning between ER protein folding, trafficking, and degradation pathways (i.e., ER quality control), cells prevent the secretion of destabilized, aggregation-prone proteins to downstream secretory environments.

In the context of systemic amyloid diseases, destabilized, amyloidogenic proteins escape ER quality control, allowing their efficient secretion to the extracellular space (Blancas-Mejia and Ramirez-Alvarado, 2013; Plate and Wiseman, 2017). This suggests that enhancing ER quality control capacity could offer a unique opportunity to reduce the aberrant secretion and toxic extracellular aggregation associated with these disorders. One strategy to improve ER quality control for amyloidogenic proteins is by activating the unfolded protein response (UPR) (Hetz and Saxena, 2017; Plate and Wiseman, 2017). The UPR regulates ER quality control through activation of UPR-associated transcription factors such as XBP1s and ATF6. These transcription factors induce overlapping, but distinct, subsets of ER chaperones, folding factors, and degradation factors (collectively ER

Please cite this article in press as: Plate et al., Quantitative Interactome Proteomics Reveals a Molecular Basis for ATF6-Dependent Regulation of a Destabilized Amyloidogenic Protein, Cell Chemical Biology (2019), https://doi.org/10.1016/j.chembiol.2019.04.001

proteostasis factors) that dictate ER quality control (Adachi et al., 2008; Lee et al., 2003; Shoulders et al., 2013; Yamamoto et al., 2004). The differential remodeling of ER quality control pathways afforded by XBP1s or ATF6 activation indicates that the independent activation of these pathways offers unique opportunities to correct pathologic defects in ER quality control for destabilized, amyloid disease-associated proteins (Plate and Wiseman, 2017).

Previous results show that stress-independent activation of XBP1s or ATF6 differentially influence ER quality control for destabilized amyloidogenic proteins such as ALLC, a destabilized Vλ6 immunoglobulin light chain (LC) associated with AL pathogenesis (Arendt et al., 2008). Stress-independent XBP1s activation increases ALLC targeting to ER degradation pathways while only modestly affecting its secretion (Cooley et al., 2014). In contrast, ATF6 activation does not increase ALLC degradation but significantly reduces the secretion and extracellular aggregation of ALLC. It does so without affecting secretion of an energetically normal Vλ6 LC or the endogenous secretory proteome (Cooley et al., 2014; Plate et al., 2016). ATF6 activation also selectively reduces the secretion and toxic aggregation of destabilized variants of other aggregation-prone proteins without significantly affecting secretion of the wild-type protein (Chen et al., 2014; Chiang et al., 2012; Shoulders et al., 2013; Smith et al., 2011b). These results identify ATF6 as a potential therapeutic target that can be pharmacologically accessed to improve ER quality control and selectively reduce the secretion and subsequent aggregation of destabilized, amyloidogenic proteins implicated in amyloid disease pathogenesis (Plate and Wiseman, 2017).

Despite this potential, the molecular mechanism responsible for ATF6-dependent reductions in destabilized, amyloidogenic protein secretion remains poorly defined. Quantitative affinity-purification mass spectrometry (q-AP-MS) has proved a powerful tool to identify changes in protein-protein interactions induced by genetic or environmental perturbations (Hosp et al., 2015; Huttlin et al., 2015; Katrina Meyer, 2015). This indicates that q-AP-MS provides a unique opportunity to define proteins and pathways responsible for dictating the selective, ATF6-dependent reduction in amyloidogenic LC secretion. Here, we implement a tandem mass tag (TMT)-based q-AP-MS platform to define how ATF6 activation improves ER quality control to selectively reduce secretion of the destabilized, amyloidogenic LC, ALLC. We demonstrate that this platform allows efficient multiplexed quantification of ALLC interaction changes induced by activation of different UPR-associated transcriptional programs. Using this TMT-based q-AP-MS approach, we show that ATF6 activation reduces ALLC secretion by increasing its targeting to ATF6-regulated ER chaperones that selectively retain this destabilized LC within the ER lumen. Overexpression of these ATF6-regulated ER chaperones only partially mimics the reduction in ALLC observed following ATF6 activation. This indicates that ATF6 activation improves LC ER quality by global remodeling of the ER proteostasis environment and not through upregulation of a specific chaperone. Our results define a mechanistic framework that explains the ATF6-dependent regulation of LC ER quality control and further motivates the development of therapeutic strategies that enhance ER quality control to ameliorate amyloid pathology in AL and related amyloid diseases.

RESULTS

A TMT-Based AP-MS Platform to Define ER Proteostasis Factors that Interact with LCs

ER quality control processes are governed by interactions between non-native protein conformations and ER proteostasis factors (Kim et al., 2013; Powers et al., 2009; Wiseman et al., 2007). Thus, defining the molecular interactions between destabilized, amyloidogenic proteins and ER proteostasis factors allows identification of the components of specific biological pathways responsible for dictating ER quality control for a given protein under defined conditions, such as ATF6 activation. However, many challenges exist in defining interactions between ER proteostasis factors and destabilized protein substrates. These include the transient nature of substrate interactions with ER proteostasis factors and the difficulty in multiplexing interactome profiling to improve throughput without sacrificing sensitivity (Budayeva and Cristea, 2014; Kean et al., 2012; Miteva et al., 2013; Pankow et al., 2015, 2016; Taipale et al., 2014).

To address these challenges in the context of amyloidogenic LCs such as ALLC, we implemented an affinity-purification mass spectrometry (AP-MS) platform that utilizes TMTs. The TMT reagents enable multiplexed quantification of changes in protein abundances across multiple conditions or biological replicates within a single MS experiment (Huttlin et al., 2015; McAlister et al., 2012, 2014; Papachristou et al., 2018; Roumeliotis et al., 2017). We utilized the platform to define the specific ER proteostasis factors important for ATF6-dependent regulation of LC ER quality control (Figure 1A). For these experiments, we employed HEK293^{DAX} cells (Shoulders et al., 2013), which exhibit ATF6-dependent reductions in the secretion of destabilized ALLC (Arendt et al., 2008), but not the energetically normal Vλ6 LC JTO (Cooley et al., 2014; Wall et al., 1999). ALLC exhibits both reduced thermodynamic stability and a faster rate of unfolding compared with JTO, which could explain the difference in amyloidogenicity (Cooley et al., 2014; Morgan and Kelly, 2016). We transiently transfected HEK293^{DAX} cells with FLAG-tagged ALLC (^{FT}ALLC), FLAG-tagged JTO (^{FT}JTO), or an untagged ALLC (Figures 1B and S1A). We previously showed that the presence of the FLAG tag does not influence ER proteostasis of LCs (Cooley et al., 2014). We subjected cells expressing these different LCs to *in situ* crosslinking using the cell-permeable crosslinker dithiobis(succinimidyl propionate) (DSP) (Lomant and Fairbanks, 1976; Nittis et al., 2010; Smith et al., 2011a). We optimized DSP crosslinking to stabilize known interactions between ER proteostasis factors (e.g., BiP) and LCs in the ER (Figures S1B and S1C). After crosslinking, we immunopurified ^{FT}ALLC or ^{FT}JTO using anti-FLAG beads. Following stringent washing in high-detergent RIPA buffer to remove non-specific interactors, the samples were reduced to cleave the disulfide bond comprising the crosslinks, alkylated, and digested with trypsin. The digested peptides arising from individual experiments were then labeled with distinct TMT reagents, combined, and analyzed by multi-dimensional protein identification technology (MuDPIT) proteomics (Washburn et al., 2001; Yates et al., 2009). Specific recovery of peptides under different

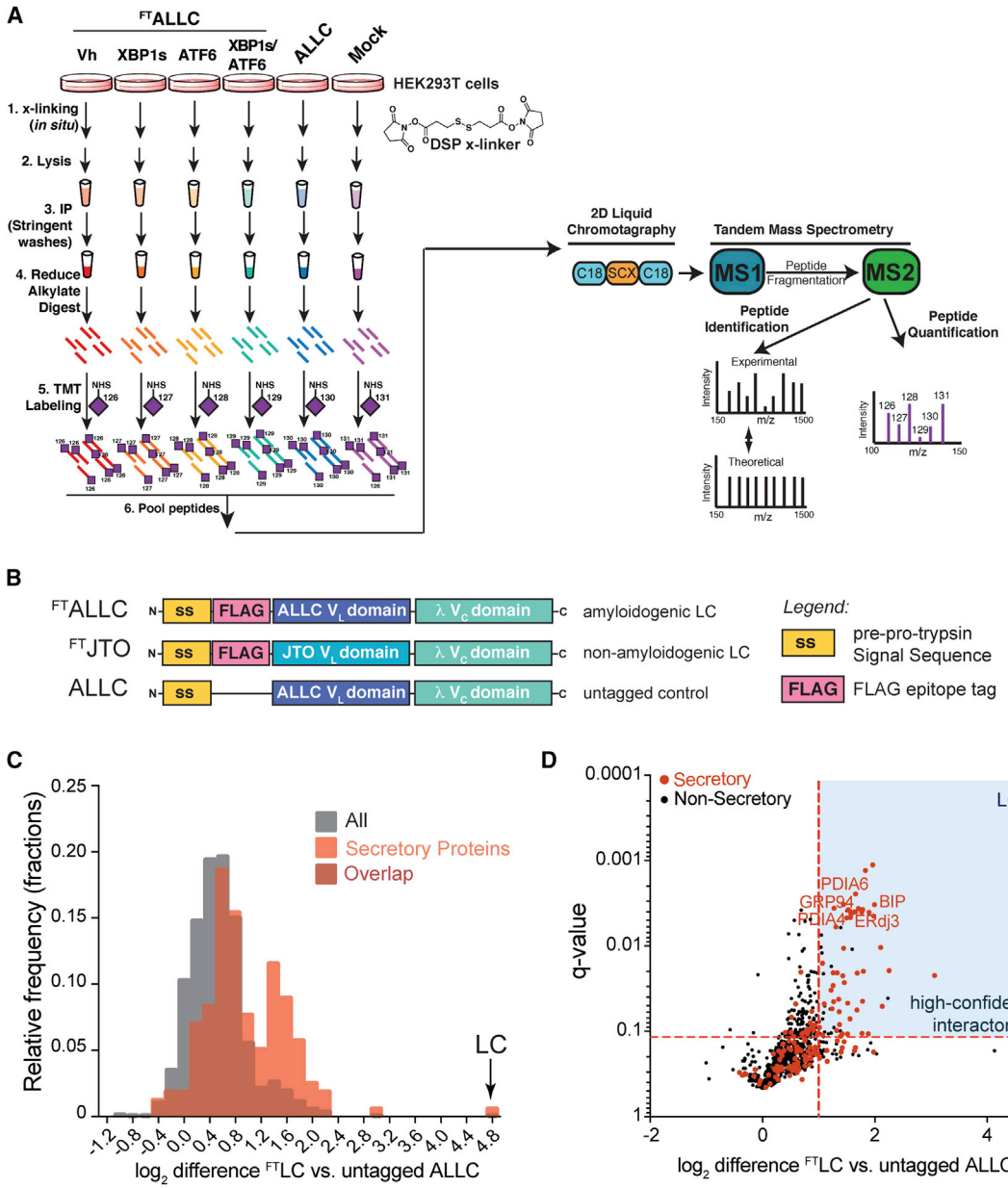

Figure 1. Establishing an AP-MS Platform to Identify ER Proteostasis Factors that Interact with Destabilized, Amyloidogenic ALLC

(A) Schematic of the multiplexed quantitative interactomics methodology, which combines affinity-purification mass spectrometry (AP-MS) with *in situ* DSP crosslinking to capture transient, low-affinity interactions with proteostasis network components. Sixplex tandem mass tags (TMT) are used for relative quantification of proteins in individual AP samples, followed by MuDPIT (2D LC coupled to tandem mass spectrometry).

(B) Illustration showing the domain organization for the FLAG-tagged destabilized, amyloidogenic LC ALLC (^{FT}ALLC), the FLAG-tagged energetically normal LC JTO (^{FT}JTO), and untagged ALLC. A sequence alignment of ALLC and JTO showing the differences in amino acid sequence is shown in Figure S1A.

(C) Histogram displaying TMT ratios of ^{FT}LC (combined n = 4 ^{FT}ALLC and n = 6 ^{FT}JTO replicates) versus untagged ALLC (mock) channels for all protein (gray) and filtered secretory protein (red).

(D) Plot showing TMT ratio ($\log_2$ difference ^{FT}LC versus untagged ALLC) versus q value (Storey) for proteins that co-purify with ^{FT}LC (either ^{FT}ALLC or ^{FT}JTO) compared with untagged ALLC in anti-FLAG IPs (n = 10 biological replicates; n = 4 for ^{FT}ALLC and n = 6 for ^{FT}JTO). High-confidence interactors are identified in the blue quadrant showing TMT ratio >2 and a q value <0.11. Secretory proteins are shown in red. Full data are included in Table S1.

conditions was then quantified by comparing the recovered signals from the TMT reporter ions in the MS2 spectra (Figure 1A).

Initially, we used this AP-MS platform to identify the ER quality control factors that bind LCs *in situ* by comparing TMT ratios for proteins that co-purify in anti-FLAG immunopurifications (IPs) from lysates prepared using HEK293^{DAX} cells expressing untagged ALLC or either ^{FT}ALLC or ^{FT}JTO (collectively ^{FT}LC). We defined the TMT ratio as: (TMT signal ^{FT}LC IPs)/(TMT signal in untagged ALLC IPs). We observed two populations of proteins isolated in these samples separated by their TMT ratio (Figure 1C

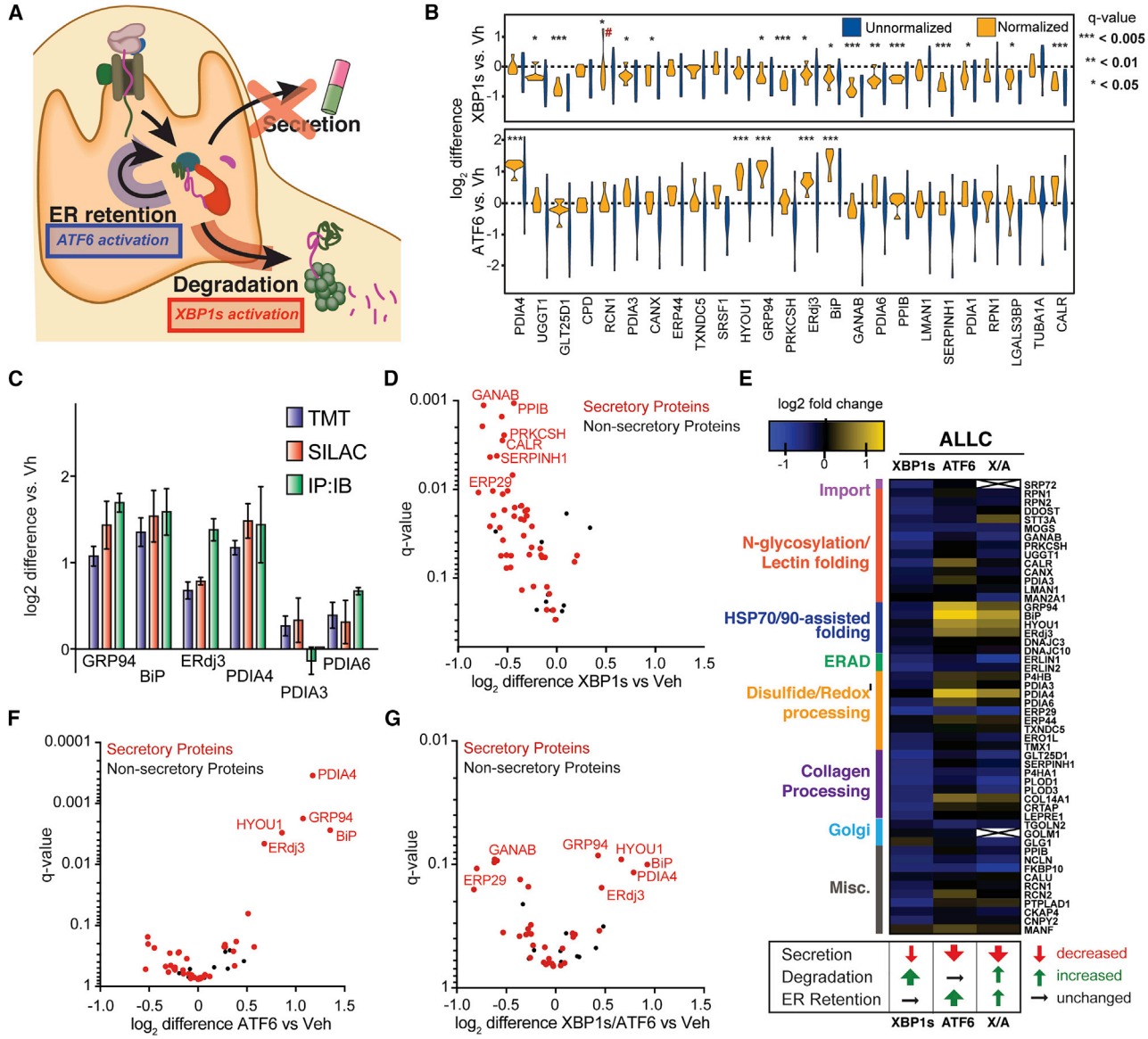

Figure 2. Stress-Independent XBP1s or ATF6 Activation Differentially Influence Interactions between ^{FT}ALLC and ER Proteostasis Factors

(A) Illustration summarizing previous data showing how stress-independent activation of XBP1s (red) or ATF6 (blue) leads to reduced secretion of destabilized, amyloidogenic ALLC (Cooley et al., 2014). XBP1s activation modestly reduces ALLC secretion through increased targeting to degradation, while ATF6 activation significantly reduces ALLC secretion through its increased ER retention.

(B) Plot showing the distribution of unnormalized (blue) and ^{FT}ALLC-bait-normalized (orange) TMT interaction ratios for n = 7 biological replicates comparing the recovery of high-confidence ALLC-interacting proteins in anti-FLAG IPs from cells following XBP1s activation (top) or ATF6 activation (bottom). A simple normalization procedure of the protein TMT signal against the ^{FT}ALLC bait protein signal across each TMT channel greatly diminishes the variance in interaction ratios. *q value (Storey) <0.15; **p < 0.05, ***p < 0.01; hash denotes excluded outlier.

(C) Comparison of interaction fold changes between ^{FT}ALLC and selected proteostasis factors in response to XBP1s or ATF6 activation as quantified by three independent methods: TMT-based q-AP-MS (n = 7 biological replicates), SILAC-based q-AP-MS (n = 4 or 5 biological replicates), or co-immunoprecipitation followed by quantitative immunoblotting (IP:IB; n = 3–6 biological replicates).

(D) Plot showing TMT interaction ratio versus q value (Storey) for high-confidence ^{FT}ALLC-interacting proteins that co-purify with ^{FT}ALLC in HEK293^{DAX} cells following stress-independent XBP1s activation from n = 7 biological replicates. Full data are included in Table S2.

(E) Heatmap displaying the observed interactions changes between ^{FT}ALLC and high-confidence ER proteostasis network components following stress-independent XBP1s or ATF6 activation (data from n = 7 biological replicates for ATF6 or XBP1s activation, and n = 4 for XBP1s/ATF6 co-activation). Interactors are organized by pathway or function. The previously defined impact of activating these pathways on ALLC secretion, degradation, and ER retention is shown below (Cooley et al., 2014).

(legend continued on next page)

and Table S1). The first population exhibits a low TMT ratio of ~1.3, which represents proteins that non-specifically co-purify in both ^{FT}LC and untagged ALLC anti-FLAG IPs. However, a second population of 72 proteins displayed a ratio of >2, indicating selective interaction with ^{FT}ALLC and ^{FT}JTO. This second population was highly enriched for secretory proteins (51 out of 72, based on gene ontology terms describing localization in the secretory pathway) and included ER proteostasis factors known to interact with LCs in the ER such as BiP, GRP94, ERdj3, HYOU1, and PDIA1 (Behnke et al., 2015, 2016; Cole et al., 2018; Davis et al., 1999; Hellman et al., 1999; Hsu et al., 1996; Melnick et al., 1992, 1994; Shen and Hendershot, 2005; Skowronek et al., 1998). We defined these 72 interacting proteins as "high-confidence interactors" of ^{FT}LC (Figure 1D), and used these proteins as the basis for subsequent AP-MS experiments focused on defining the ER quality control pathways responsible for the selective, ATF6-dependent regulation of ALLC secretion.

TMT-Based Q-AP-MS Allows Multiplexed Quantification of ALLC Interaction Changes Induced by XBP1s and/or ATF6 Activation

To define the specific ER proteostasis factors responsible for the differential impact of ATF6 or XBP1s activation on ALLC ER quality control (Figure 2A), we used our TMT-based q-AP-MS proteomic platform to identify high-confidence interactors that show altered interaction with ^{FT}ALLC following stress-independent activation of these UPR-associated transcription factors in HEK293^{DAX} cells. These cells express both doxycycline (dox)-inducible XBP1s and a trimethoprim (TMP)-regulated DHFR.ATF6, allowing stress-independent XBP1s or ATF6 activation through the administration of dox or TMP, respectively (Shoulders et al., 2013). We compared the recovery of TMT signals for high-confidence LC interactors that co-purify with ^{FT}ALLC in lysates prepared from HEK293^{DAX} cells following 24-h treatment with vehicle, dox (activates XPB1s), or TMP (activates ATF6)—a treatment paradigm we previously showed is sufficient to induce efficient remodeling of ER proteostasis pathways (Shoulders et al., 2013). A challenge in comparing the TMT signals across different IPs is the variability of bait protein (e.g., ^{FT}ALLC). ^{FT}ALLC can vary in concentration owing to factors including differences in transfection across biological replicates, variability in sample preparation, or alterations in protein secretion or degradation caused by XBP1s and/or ATF6 activation (Cooley et al., 2014). This results in a large variance in unnormalized interaction ratios for high-confidence interactors (Figures 2B [blue] and S2A). To address this variability, we normalized the recovery of high-confidence interactors to the amount of ^{FT}ALLC identified in each channel. Normalization significantly improved the variance across samples (Figure 2B, orange) and allowed quantification of interaction changes using this approach. Importantly, we showed high reproducibility of ^{FT}ALLC-interaction changes induced by XBP1s or ATF6 activation across seven independent biological replicates (Figures S2B and S2C).

TMT-based quantification of proteomics data is challenged in complex proteomes by reporter ion ratio compression. This is caused by co-isolation of interfering precursor ions and subsequent co-fragmentation, resulting in an underestimation of the abundance ratios (Savitski et al., 2013; Ting et al., 2011). Synchronous precursor selection (SPS) MS3 analysis is commonly employed to overcome this ratio compression challenge; however, this analysis is only possible using specialized Tribrid MS instruments, such as the Fusion Lumos (Huttlin et al., 2015; McAlister et al., 2014; Papachristou et al., 2018; Roumeliotis et al., 2017). Due to the simplicity of our proteomes afforded by the AP isolation of ^{FT}ALLC, we predicted that ratio compression would be minimized and allow accurate quantification using MS2 reporter ion quantification. Furthermore, we performed our analysis using MuDPIT, which increases the chromatographic separation of peptides—another parameter that has been shown to reduce TMT ratio compression (Ow et al., 2011). To ensure that ratio compression is minimized, we compared ^{FT}ALLC-interaction ratios for high-confidence interactors measured by TMT-based proteomics with ratios determined using stable isotope labeling with amino acids in cell culture (SILAC), an independent quantitative proteomics approach that relies on quantification of light- and heavy-isotope-labeled precursor ions in the MS1 spectra (Figure S2D) (Ong et al., 2002). As with TMT-based AP-MS, we performed SILAC-based AP-MS to monitor changes in ^{FT}ALLC interactome induced by XBP1s and/or ATF6 activation in HEK293^{DAX} cells (Figures S2D–S2F). Alterations in the interactions between ER proteostasis factors and ^{FT}ALLC observed using the alternative SILAC-based quantitation were nearly identical to those obtained using TMT-based quantification (Figures S2G). To further confirm the accuracy of our TMT-quantification AP-MS assay, we confirmed XBP1s- or ATF6-dependent interaction changes between ^{FT}ALLC and selected high-confidence interactors using AP followed by quantitative immunoblotting (IP:IB) (Figures 2C and S2H). This proteomic-independent approach showed similar interaction ratio changes. Collectively, these results show that our TMT-based AP-MS platform can accurately monitor changes in the ^{FT}ALLC interactome induced by XBP1s and/or ATF6 activation.

Comparing our multiplexed TMT-based interatomic approach with SILAC quantification also demonstrated enhanced throughput capacity. Since SILAC quantification only enables binary comparisons, a higher number of MS runs and more instrument time was needed to generate the quantitative comparisons between different conditions (Figures S2I and S2J). Furthermore, the number of proteins that could be reliably quantified in at least three biological replicates was at least 4-fold greater using our TMT-based platform than in any of the pairwise SILAC comparisons (Figures S2K and S2L). The improved analysis time and more reliable protein identification in our TMT-based AP-MS platform highlights an additional advantage of this platform over more commonly used label-free or SILAC-based approaches for defining interactome changes for destabilized

(F) Plot showing TMT interaction ratio versus q value (Storey) for high-confidence ^{FT}ALLC-interacting proteins that co-purify with ^{FT}ALLC in HEK293^{DAX} cells following stress-independent ATF6 activation from n = 7 biological replicates. Full data are included in Table S2.

(G) Plot showing TMT interaction ratio versus q value (Storey) for high-confidence ^{FT}ALLC-interacting proteins that co-purify with ^{FT}ALLC in HEK293^{DAX} cells following stress-independent XBP1s and ATF6 co-activation from n = 4 biological replicates. Full data are included in Table S2.

proteins such as ^{FT}ALLC in response to selective ATF6 or XBP1s activation.

XBP1s or ATF6 Activation Differentially Influences Interactions between ER Quality Control Factors and ^{FT}ALLC

Stress-independent activation of XBP1s or ATF6 differentially influence ALLC ER quality control (Figure 2A) (Cooley et al., 2014). XBP1s activation increases targeting of ALLC to degradation while only modestly reducing ALLC secretion. In contrast, ATF6 activation significantly reduces ALLC secretion and subsequent aggregation by >50% but does not increase ALLC degradation, indicating that activating ATF6 increases the ER retention of this destabilized LC. To define the specific ER proteostasis factors responsible for the differential impact of ATF6 or XBP1s activation on ALLC ER quality control, we compared the changes in the ^{FT}ALLC interactome induced by XBP1s and/or ATF6 activation.

Interestingly, XBP1s or ATF6 activation induce distinct changes in the interactions between ^{FT}ALLC and ER proteostasis factors, reflecting the distinct impact of these UPR-associated transcription factors on ALLC ER quality control (Figures 2D–2F and Table S2) (Cooley et al., 2014). XBP1s activation globally reduces interactions between ^{FT}ALLC and ER proteostasis factors (Figures 2D and 2E). This is consistent with the XBP1s-dependent increase in ALLC targeting to ER degradation pathways such as ERAD or autophagy, the latter being the predominant pathway responsible for degrading ALLC following ER stress (Cooley et al., 2014). Unfortunately, components of degradation pathways were poorly detected in our proteomics samples, which likely reflects poor crosslinking between ERAD factors and ^{FT}ALLC or that these mainly membrane-associated proteins require specific detergents for solubilization (Christianson et al., 2011). In contrast, ATF6 activation increases interactions between ^{FT}ALLC and select ER proteostasis factors, including the ATP-dependent ER chaperones BiP and GRP94, the BiP co-chaperones ERdj3 and HYOU1, and the protein-disulfide isomerase PDIA4 (Figures 2E and 2F). The increase in ^{FT}ALLC interactions with these ER proteostasis factors is consistent with the ATF6-dependent increase in ALLC ER retention (Cooley et al., 2014) and suggests that ATF6 activation reduces secretion of ALLC through the increased targeting of this destabilized LC to specific ER proteostasis pathways.

Despite affecting ALLC ER quality control through distinct mechanisms, co-activation of XBP1s and ATF6 does not synergistically influence destabilized ALLC secretion (Cooley et al., 2014). Instead, XBP1s and ATF6 co-activation reduces ALLC secretion to the same extent observed with ATF6 activation alone and modestly increases ALLC degradation (Cooley et al., 2014). This indicates that co-activation of these transcription factors integrates distinct functional aspects of independent XBP1s or ATF6 activation to influence ALLC ER quality control. Consistent with this, AP-MS shows that XBP1s and ATF6 co-activation remodels the ^{FT}ALLC interactome by promoting specific changes also observed following independent transcription factor activation (Figures 2E and 2G; Table S2). For example, XBP1s and ATF6 co-activation reduces interactions between ^{FT}ALLC and numerous high-confidence interactors, consistent with the moderate increase in ALLC degradation observed under these conditions (Cooley et al., 2014). Alternatively, co-activation of these transcription factors increases interactions between ^{FT}ALLC and ER proteostasis factors including BiP, GRP94, ERdj3, HYOU1, and PDIA4, all of which are also increased following ATF6 activation alone.

Comparing the functional impact of XBP1s and/or ATF6 activation on ALLC ER quality control with the changes in the interactions between ^{FT}ALLC and ER proteostasis pathways provides an opportunity to identify the ER proteostasis factors likely responsible for the regulation of ALLC secretion. ATF6 activation, in both the presence and absence of XBP1s activation, reduces ALLC secretion by 50% (Cooley et al., 2014). Based on our AP-MS analysis, this reduced secretion corresponds to increased interactions with a specific subset of ER proteostasis factors including BiP, GRP94, HYOU1, ERdj3, and PDIA4. We confirmed the ATF6-dependent increase in the interactions between these ER proteostasis factors and ^{FT}ALLC by IP:IB (Figure 2C). This suggests that these proteostasis factors are involved in dictating the selective, ATF6-dependent reduction in destabilized ALLC secretion.

ATF6 Activation Increases the Interactions between ER Proteostasis Factors and an Energetically Normal LC

ATF6 activation selectively reduces secretion of destabilized ALLC relative to the energetically normal LC JTO (Cooley et al., 2014). Thus, we sought to define how ATF6 activation influences the interactions between JTO and ER proteostasis factors. Initially, we directly compared the interactomes of ^{FT}ALLC and ^{FT}JTO in vehicle-treated HEK293^{DAX} cells using our AP-MS proteomic platform (Figure 1A). To normalize the recovery of ER proteostasis factors in these IPs, we used peptides from the λ V_c domain of these LCs, which is identical between ALLC and JTO (Figure S1A). This allowed us to accurately monitor the differential interactions between ER proteostasis factors and specific LCs in this experiment (Figure 3A). Using this approach, we identified numerous high-confidence LC-interacting proteins that showed increased association with the destabilized ALLC, relative to the stable JTO (Figures 3A and S3A; Table S3). This includes many ER proteostasis factors identified to increase association upon ATF6 activation such as BiP and GRP94, indicating that these proteins are key determinants in dictating LC ER quality control. We confirmed the increased association of select ER proteostasis factors with ALLC by IP:IB (Figure S3B).

Next, we evaluated how ATF6 activation influences the interactions between ^{FT}JTO and ER proteostasis factors. ATF6 activation induced a remodeling of the ^{FT}JTO interactome similar to that observed for ^{FT}ALLC (Figures 3B, 3C, and S3C; Table S3). These results indicate that ATF6-dependent increases in the interactions with ER proteostasis factors occur independent of the energetic stability of the LC. However, interactions between ER proteostasis factors and ^{FT}JTO after ATF6 activation are nonetheless lower than observed for ^{FT}ALLC because basal ^{FT}JTO interactions are fewer compared with ^{FT}ALLC (Figures 3A, S3A, and S3B). This indicates that increased targeting of ^{FT}ALLC to specific ER proteostasis factors likely represents a molecular mechanism responsible for selective, ATF6-dependent retention of this destabilized LC sequence.

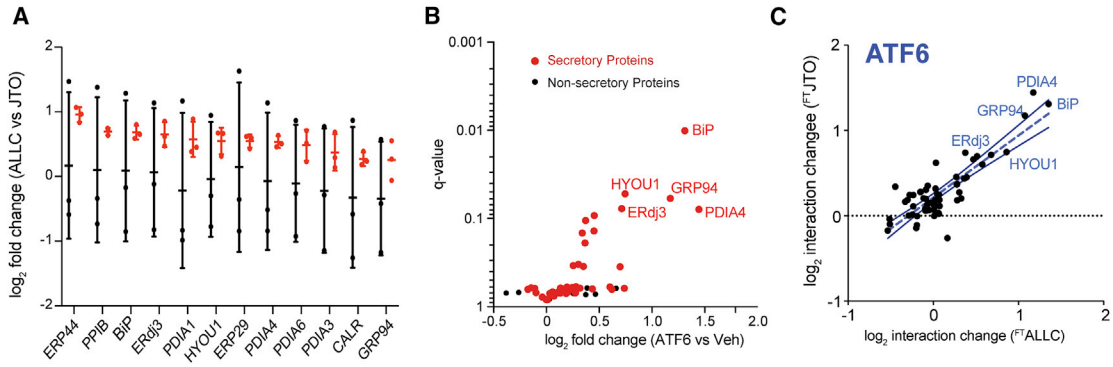

Figure 3. ATF6 Activation Increases Interactions between Non-amyloidogenic ^{FT}JTO and ER Proteostasis Factors

(A) Distribution of unnormalized (black) and normalized (red) TMT ratios of ^{FT}ALLC versus ^{FT}JTO for proteins with significant interaction changes (n = 3 biological replicates). Peptides of the λ V_c domain, which is identical for ALLC and JTO (Figure S1A), were used to normalize the TMT signal of each individual protein against the λ V_c domain peptide signal across each TMT channel.

(B) Plot showing TMT interaction ratio versus q value for high-confidence ALLC-interacting proteins that co-purify with ^{FT}JTO from HEK293^{DAX} cells following treatment with vehicle or TMP (to activate ATF6) for 16 h (n = 6 biological replicates). Secretory proteins are shown in red. Full data are available in Table S3.

(C) Plot comparing the interaction changes of high-confidence ALLC-interacting proteins with either ^{FT}ALLC (n = 7 biological replicates) or ^{FT}JTO (n = 6 biological replicates) following stress-independent ATF6 activation. The dashed line represents least-squares linear regression. The solid lines show 95% confidence intervals.

ATF6 Transcriptionally Regulates ER Proteostasis Factors that Show Increased Interactions with ^{FT}ALLC

ATF6 activation transcriptionally regulates the expression of multiple ER proteostasis factors that show increased association with ^{FT}ALLC following stress-independent ATF6 activation (e.g., BiP, GRP94) (Shoulders et al., 2013; Yamamoto et al., 2004). This suggests that the increased interaction between these ER proteostasis and ^{FT}ALLC is regulated by ATF6-dependent increases in ER proteostasis factor expression. Consistent with this, ATF6-dependent changes in mRNA for high-confidence interactors correlate with changes in interactions with ^{FT}ALLC (Figure 4A and Table S4) (Plate et al., 2016). A similar relationship was observed when we compared ATF6-dependent increases in the protein levels for these ER proteostasis factors (measured by whole-cell quantitative proteomics [Plate et al., 2016]) with increases in ^{FT}ALLC interactions (Figure 4B). These results indicate that the increased interactions between ^{FT}ALLC and ER proteostasis factors are primarily dictated by ATF6-dependent increases in their expression.

Despite this general correlation, increased expression of ER proteostasis factors does not appear sufficient to increase ^{FT}ALLC interactions. This is evident by monitoring the recovery of the high-confidence LC interactor DNAJC3 in ^{FT}ALLC IPs (Figures 4A and 4B). DNAJC3 is an ER HSP40 co-chaperone that binds to misfolded proteins within the ER and directs them to the ER HSP70 BiP for ATP-dependent chaperoning (Petrova et al., 2008; Rutkowski et al., 2007). ATF6 activation increases the expression of DNAJC3 more than 2-fold; however, we observe no significant increase in the association between DNAJC3 and ^{FT}ALLC by AP-MS (Figures 4A, 4B, and S4A). This suggests that while ATF6-dependent increases in the expression of ER proteostasis factors such as BiP or GRP94 are important for dictating their increased interactions with ^{FT}ALLC, increased expression does not appear sufficient to increase these interactions.

ATF6 and XBP1s induce overlapping, but distinct, subsets of ER proteostasis factors (Shoulders et al., 2013; Yamamoto et al., 2004). This provides a unique opportunity to identify key ER proteostasis factors specifically required for ATF6-dependent reductions in ALLC secretion. Toward that aim, we compared XBP1s-dependent changes in ER proteostasis factor expression with changes in their interaction with ^{FT}ALLC. Unlike what we observed with ATF6 activation, XBP1s-dependent ER proteostasis factor expression does not correlate with ^{FT}ALLC interactions (Figure 4C). However, co-activation of XBP1s and ATF6 largely restored the correlation between ER proteostasis factor expression and ^{FT}ALLC interactions (Figure 4D). Interestingly, specific ER proteostasis factors such as HYOU1 and PDIA4 were transcriptionally induced by XBP1s or ATF6 activation alone, but only showed increased interactions with ^{FT}ALLC following ATF6 activation (Figures 4E and 4F). This is in contrast to other ER proteostasis factors such as BiP and GRP94 that are primarily regulated by ATF6 and show increased association with ^{FT}ALLC following ATF6 activation (Figures S4B and S4C). The inability for XBP1s-dependent upregulation of PDIA4 and HYOU1 to increase interactions with ^{FT}ALLC suggests that the increased expression of these ER proteostasis factors is not sufficient to influence LC ER quality control. Instead, these results suggest increased targeting to ATF6-regulated, ATP-dependent chaperones such as BiP and GRP94 is primarily responsible for the ATF6-dependent increase in LC ER quality control.

Overexpression of Specific ER Proteostasis Factors Recapitulates Selective, ATF6-Dependent Reductions in Destabilized LC Secretion

Many of the ER proteostasis factors found to increase interactions with destabilized ^{FT}ALLC following ATF6 activation (e.g., BiP, GRP94, and ERdj3) were previously reported to function as "pro-folding" factors for LCs within the ER. BiP and GRP94 function sequentially in the folding of LCs in the ER (Melnick et al., 1994). Furthermore, BiP and ERdj3 can bind multiple

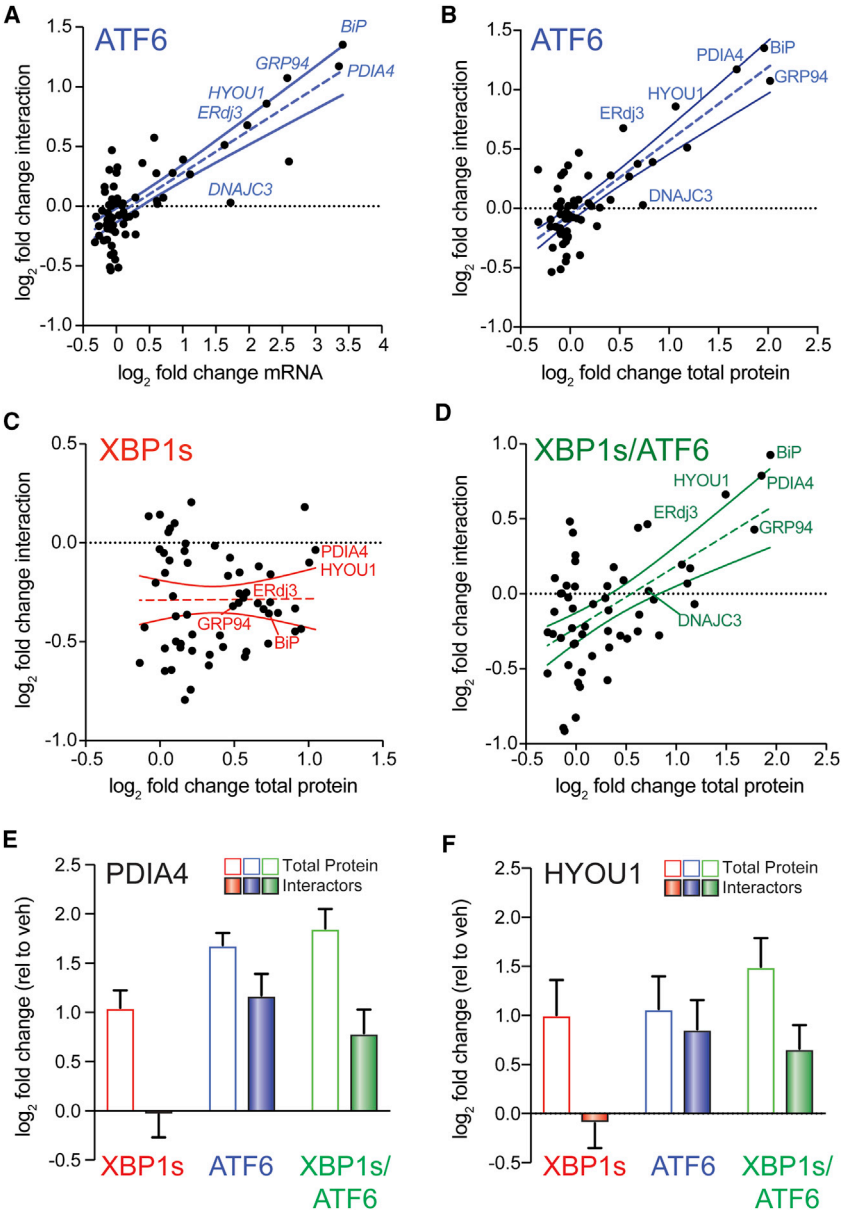

Figure 4. ATF6-Dependent Increases in ALLC Interactions Correlate with ER Proteostasis Factor Expression

(A) Plot comparing mRNA level for high-confidence ALLC-interacting proteins (measured by RNA sequencing in Plate et al., 2016; n = 3 biological replicates) versus their increased interactions with ^{FT}ALLC in HEK293^{DAX} cells following stress-independent ATF6 activation (n = 7 biological replicates). The dashed line shows least-squares linear regression. The solid lines show 95% confidence intervals.

(B) Plot comparing cellular protein level for high-confidence ALLC-interacting proteins (measured by whole-cell quantitative proteomics in Plate et al., 2016; n = 3 biological replicates) versus their increased interactions with ^{FT}ALLC in HEK293^{DAX} cells following stress-independent ATF6 activation (n = 7 biological replicates). The dashed line shows least-squares linear regression. The solid lines show 95% confidence intervals.

(C) Plot comparing cellular protein level for high-confidence ALLC-interacting proteins (measured by whole-cell quantitative proteomics in Plate et al., 2016; n = 3 biological replicates) versus their increased interactions with ^{FT}ALLC in HEK293^{DAX} cells following stress-independent XBP1s activation (n = 7 biological replicates). The dashed line shows least-squares linear regression. The solid lines show 95% confidence intervals.

(D) Plot comparing cellular protein level for high-confidence ALLC-interacting proteins (measured by whole-cell quantitative proteomics in Plate et al., 2016; n = 3 biological replicates) versus their increased interactions with ^{FT}ALLC in HEK293^{DAX} cells following stress-independent ATF6 and XBP1s co-activation (n = 4 biological replicates). The dashed line shows least-squares linear regression. The solid lines show 95% confidence intervals.

(E) Graph showing changes in protein levels (open symbols; n = 3) or ^{FT}ALLC interactions (solid bars; n = 4–7) for PDIA4 in HEK293^{DAX} cells following stress-independent XBP1s (red), ATF6 (blue), or XBP1s and ATF6 (green) activation. Error bars show SEM for the individual replicates.

(F) Graph showing changes in protein levels (open symbols; n = 3) or ^{FT}ALLC interactions (solid bars; n = 4–7) for HYOU1 in HEK293^{DAX} cells following stress-independent XBP1s (red), ATF6 (blue), or XBP1s and ATF6 (green) activation. Error bars show SEM for the individual replicates.

hydrophobic sites localized throughout a non-secreted LC, preventing its aggregation and/or premature degradation (Behnke et al., 2016). In contrast, other BiP co-chaperones such as ERdj4 and ERdj5—neither of which is regulated by ATF6 (Shoulders et al., 2013)—bind rarer, aggregation-prone sequences within the LC to increase its targeting to degradation. This indicates that ATF6 activation induces selective remodeling of ER chaperoning pathways that increase targeting of LCs to ATF6-regulated pro-folding factors.

Our results indicate that ATF6 activation increases LC targeting to these pro-folding factors by increasing their expression. Thus, we predicted that overexpression of specific pro-folding chaperones should mimic the capacity for ATF6 activation to selectively reduce secretion of destabilized, aggregation-prone LCs. To test this prediction, we co-overexpressed ^{FT}ALLC and the ATF6-regulated chaperones BiP, GRP94, or ERdj3 in HEK293^{DAX} cells and evaluated ^{FT}ALLC secretion by ELISA. In this experiment, we collected lysates and conditioned media from cells following 0 or 4 h incubation with cycloheximide (CHX) in fresh media. We then calculated the fraction of ^{FT}ALLC secreted using the equation: fraction secreted = (^{FT}ALLC medium at t = 4 h)/(^{FT}ALLC lysate at t = 0 h). Overexpression of BiP or GRP94 decreased ^{FT}ALLC fraction secreted by >20% (Figure 5A). In contrast, ERdj3 overexpression reduced ^{FT}ALLC secretion by a more modest 10%, likely reflecting the modest intracellular increase in this co-chaperone afforded by overexpression owing to its efficient secretion to the media (Genereux et al., 2015). Similar results were observed by [^{35}S] metabolic

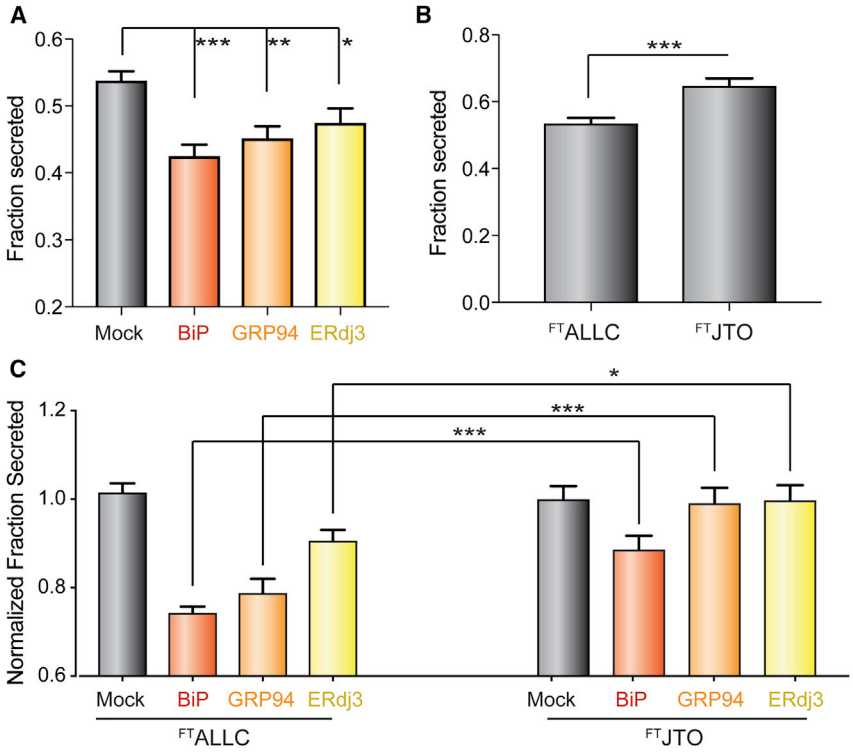

Figure 5. Overexpression of ATF6-Regulated Pro-folding ER Proteostasis Factors Preferentially Reduces ALLC Secretion

(A) Graph showing the fraction secreted for ^{FT}ALLC from HEK293^{DAX} cells overexpressing the indicated ER proteostasis factor and treated with cycloheximide (CHX) for 0 or 4 h, as measured by ELISA. Fraction secreted was quantified using the following equation: fraction secreted = (^{FT}ALLC in media at t = 4 h)/(^{FT}ALLC in lysate at t = 0 h). Error bars show SEM for n > 14 replicates across >4 independent experiments. *p < 0.05, **p < 0.01, ***p < 0.005 for unpaired t tests are shown.

(B) Graph showing fraction secretion for ^{FT}ALLC or ^{FT}JTO from HEK293^{DAX} cells treated with CHX for 0 or 4 h, as measured by ELISA. Fraction secreted was calculated as described in Figure 4A. Error bars show SEM for n > 9 replicates across n > 3 independent experiments. ***p < 0.005 for unpaired t test is shown.

(C) Graph showing the normalized fraction secreted of ^{FT}ALLC or ^{FT}JTO from HEK293^{DAX} cells overexpressing the indicated ER chaperoning factor. Normalized fraction secreted was calculated by the following equation: (fraction secretion in cells overexpressing a given chaperone)/(fraction secretion in mock-transfected cells). Fraction secreted was calculated as in Figure 4A. Error bars show SEM for n > 9 replicates collected across >3 independent experiments. *p < 0.05, ***p < 0.005 for unpaired t tests are shown.

labeling (Figures S5A and S5B). Importantly, we do not observe significant loss of ^{FT}ALLC over a 4-h time course in our [^{35}S] metabolic labeling experiment, indicating that the reduction in ^{FT}ALLC secretion observed upon overexpression of ER chaperones does not correspond to an increase in degradation (Figure S5C). This result is identical to that observed upon ATF6 activation and indicates that overexpression of ER chaperones attenuates ALLC secretion through the same ER retention mechanism afforded by ATF6 activation (Cooley et al., 2014).

ATF6 activation selectively reduces secretion of destabilized, amyloidogenic ALLC relative to the energetically normal, non-amyloidogenic JTO. Thus, we sought to define whether overexpression of BiP, GRP94, or ERdj3 influenced secretion of ^{FT}JTO using our ELISA assay (Cooley et al., 2014; Plate et al., 2016). ALLC and JTO are secreted from cells with different secretion efficiencies, reflecting differences in the ER quality control for LCs with distinct stabilities (Cooley et al., 2014), a difference further supported herein by the differential interactions between these LCs and ER proteostasis factors defined by our AP-MS analysis (Figures 3A, S3A, and S3B). Consistent with this, we found that the fraction of ALLC secreted measured by CHX/ELISA is less than that observed for the more stable JTO (Figure 5B). Thus, to compare the secretion of ALLC and JTO in cells also overexpressing specific ER proteostasis factors, we normalized the secretion of these two LCs to control cells overexpressing each LC alone. Using this approach, we show that overexpression of BiP modestly reduces ^{FT}JTO secretion; however, this reduction is significantly less than that observed for ^{FT}ALLC (Figure 5C). Alternatively, despite significantly reducing ^{FT}ALLC secretion, neither GRP94 nor ERdj3 overexpression affects ^{FT}JTO secretion (Figure 5C). These results show that overexpression of these ER proteostasis factors preferentially reduces secretion of the destabilized, amyloidogenic ALLC, mirroring the improved LC ER quality control observed upon ATF6 activation (Cooley et al., 2014).

BiP Overexpression Only Partially Recapitulates the ATF6-Dependent Reduction in ALLC Secretion

RNAi depletion of core ER chaperones such as BiP or GRP94 activates the UPR, preventing us from defining the importance of these ER proteostasis factors for the ATF6-dependent reduction in destabilized ALLC secretion (Cooley et al., 2014). Instead, we evaluated how overexpression of the ATF6-regulated ER chaperone BiP influences ALLC secretion in the presence or absence of ATF6 activation. We selected BiP for this experiment because it is a core ER proteostasis factor whose overexpression reduces ALLC secretion to the greatest extent (Figure 5C). Interestingly, the 20% reduction in ALLC secretion afforded by BiP overexpression is significantly less than the 40% reduction in secretion observed following ATF6 activation (Figure 6A). The combination of BiP overexpression and ATF6 activation shows no further reduction in destabilized ALLC secretion as compared with ATF6 activation alone (Figure 6A). Similar results were observed by [^{35}S] metabolic labeling whereby we showed that the rate of ALLC secretion observed by ATF6 activation is less than that observed following BiP overexpression (Figures 6B and S6A–S6C). These results indicate that overexpression of a core ER proteostasis factors only partially mimics the improved LC ER quality control observed following ATF6 activation and suggests that maximal reductions in ALLC secretion can only be achieved upon global, ATF6-dependent remodeling of ER quality control pathways.

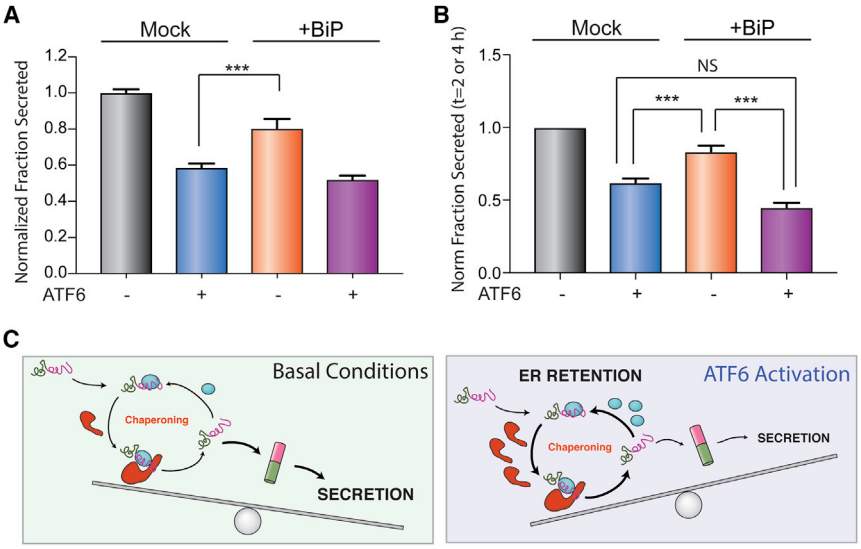

Figure 6. Overexpression of BiP Partially Recapitulates ATF6-Dependent Reductions in ALLC Secretion

(A) Graph showing the normalized fraction secretion of ^{FT}ALLC in HEK293^{DAX} cells mock transfected or overexpressing *BiP* subjected to a 16-h pretreatment with vehicle or ATF6 activation, as measured by ELISA. ATF6 was activated in these cells using trimethoprim (TMP; 10 μM), as previously described (Shoulders et al., 2013). Error bars show SEM for n = 6 replicates across two independent experiments. ***p < 0.005 for unpaired t test.

(B) Graph showing the normalized fraction secretion of ^{FT}ALLC at t = 2 or 4 h in HEK293^{DAX} cells mock transfected or overexpressing *BiP* subjected to 16-h pretreatment with vehicle or ATF6 activation, as measured by [^{35}S] metabolic labeling. Representative autoradiograms are included in Figure S6A. Error bars show SEM for n = 4 separate measurements (2 measurements at t = 2 h and 2 measurements at t = 4 h) across two independent experiments. *p < 0.05, ***p < 0.005 for paired t test.

(C) Illustration showing a molecular model that explains the selective, ATF6-dependent reduction in destabilized ALLC secretion. The increased chaperoning environment afforded by ATF6 activation promotes iterative rounds of ALLC chaperoning to reduce ALLC folding into a trafficking competent conformation. This leads to increased ER retention of destabilized ALLC in chaperone-bound complexes that prevent its secretion to downstream secretory environments.

DISCUSSION

Here, we show that ATF6 activation improves ER quality control for destabilized LCs through increased targeting to select "pro-folding" ER proteostasis factors. Interestingly, despite the fact that activating ATF6 selectively reduces secretion of destabilized LCs, ATF6 activation increases interactions between pro-folding ER proteostasis factors and both destabilized (e.g., ALLC) and stable (e.g., JTO) LCs. This suggests that the increased activity of these pro-folding factors improves their capacity to "read out" the energetic stability of LCs and more efficiently regulate their ER quality. A potential explanation for this effect is that increased targeting to pro-folding ER proteostasis factors increases iterative rounds of chaperone-assisted folding that selectively prevents destabilized, amyloidogenic LCs such as ALLC from adopting a secretion-competent conformation (Figure 6C). In this model, destabilized ALLC is unable to complete its folding upon release from ER chaperoning pathways. Instead, the enhanced activity of these proteostasis factors afforded by ATF6 activation promotes re-engagement of ALLC prior to folding, preventing trafficking to downstream secretory environments. This re-engagement of destabilized ALLC with pro-folding factors similarly prevents targeting to degradation pathways, resulting in the ER retention observed following ATF6 activation (Cooley et al., 2014). In contrast, energetically normal LCs such as JTO can efficiently fold following release from chaperoning pathways in the ATF6-remodeled ER environment due to its increased stability relative to ALLC (Cooley et al., 2014; Morgan and Kelly, 2016). This allows JTO to adopt a trafficking-competent conformation that can then be secreted to the extracellular space. Thus, while ATF6 activation increases interactions between JTO and select ER proteostasis factors, the capacity for this energetically normal LC to fold following release from ER chaperones prevents ATF6 activation from significantly impairing its secretion. This indicates that the selective, ATF6-mediated remodeling of pro-folding LC chaperoning pathways provides a unique opportunity to engage non-native LC conformations through interactions with multiple ER chaperones and co-chaperones to selectively reduce secretion of destabilized LCs implicated in AL disease pathogenesis.

Interestingly, overexpression of specific ER chaperones such as BiP only partially mimic the increases in LC ER quality afforded by ATF6 activation. This highlights a unique advantage for targeting endogenous transcriptional signaling pathways such as ATF6 to influence ER quality control for disease-associated proteins, compared with targeting the activity of specific chaperones. The ATF6 transcriptional signaling pathway evolved to restore ER quality and function following diverse types of ER insults. As such, ATF6 regulates a distinct subset of ER proteostasis factors that can coordinate to affect ER quality control, providing an optimized environment to selectively influence the secretion of destabilized, amyloidogenic proteins such as amyloidogenic LCs. Consistent with this, our results show that ATF6 activation improves LC ER quality control to greater extents than that achieved by overexpression of specific ER proteostasis factors such as BiP or GRP94. This reflects the more global, ATF6-dependent remodeling of the ALLC interactome described herein, whereby ATF6 activation increases the interactions between ^{FT}ALLC and multiple pro-folding ER proteostasis factors.

The capacity for ATF6 activation to optimize ER proteostasis remodeling and improve LC ER quality control suggests that pharmacologic ATF6 activation provides an opportunity to reduce the secretion and subsequent aggregation of amyloidogenic LCs and other amyloidogenic proteins involved in diverse diseases (Plate and Wiseman, 2017). Interestingly, small-molecule ER proteostasis regulators that activate ATF6 in AL patient-derived plasma cell models increase

ALLC targeting to ER chaperones including BiP and GRP94 and reduce ALLC secretion (Plate et al., 2016), indicating that pharmacologic targeting of ER proteostasis can reduce ALLC secretion through a mechanism analogous to that described herein. Stress-independent ATF6 activation also reduces the secretion and toxic aggregation of destabilized variants of multiple other disease-associated proteins including TTR, rhodopsin, and α1-antitrypsin (Chen et al., 2014; Chiang et al., 2012; Shoulders et al., 2013; Smith et al., 2011b). Thus, our results defining the global remodeling of ALLC interactions afforded by ATF6 activation provide a molecular basis to deconvolute the impact of ATF6 activation on the ER quality control for these and other disease-relevant proteins. Our results also further motivate the discovery and development of pharmacologic ATF6-activating compounds that have the potential to ameliorate the aberrant secretion and toxic aggregation of destabilized, aggregation-prone proteins implicated in etiologically diverse protein-aggregation diseases (Plate and Wiseman, 2017).

SIGNIFICANCE

Remodeling of ER proteostasis pathways has emerged as a promising strategy to correct protein quality control defects associated with diverse protein misfolding diseases such as light-chain amyloidosis. In particular, remodeling ER proteostasis pathways through stress-independent activation of the unfolded protein response-associated transcription factor ATF6 has been shown to reduce secretion and extracellular aggregation of destabilized, amyloidogenic proteins, while not affecting secretion of the stable wild-type proteome. However, the molecular mechanism by which ATF6 activation influences amyloidogenic protein secretion remains poorly defined. ATF6 transcriptionally regulates a subset of ER chaperones and quality control factors, yet the molecular details of how these factors enhance ER quality control decisions and prevent the secretion of destabilized, amyloidogenic proteins has been elusive. Here, we use a multiplexed quantitative proteomics platform to define the molecular mechanism by which ATF6 activation selectively influences secretion of the destabilized, amyloidogenic immunoglobulin light chain ALLC. We show that ATF6 activation increases interactions between ALLC and ER chaperones to increase retention of this destabilized protein within the ER. These increased interactions are mediated through ATF6-dependent transcriptional upregulation of ER chaperones and reflect remodeling of ER proteostasis pathways afforded by ATF6 activation. Interestingly, overexpression of specific ATF6-regulated chaperones only partially recapitulates the reduced secretion of ALLC afforded by ATF6 activation, highlighting the benefit of global remodeling of ER proteostasis for improving ER quality control of destabilized proteins through activation of endogenous stress-responsive signaling pathways. These results inform on the utility of therapeutic strategies targeting stress-independent activation of the ATF6 pathway to reduce secretion of destabilized protein variants associated with diverse protein aggregation diseases.

STAR★METHODS

Detailed methods are provided in the online version of this paper and include the following:

- KEY RESOURCES TABLE
- CONTACT FOR REAGENT AND RESOURCE SHARING
- EXPERIMENTAL MODEL AND SUBJECT DETAILS
  - Cell Culture and Transfections
- METHOD DETAILS
  - Plasmids and Antibodies
  - Affinity-Purification of LC Samples and MS Sample Preparation
  - Mass Spectrometry and Interactome Characterization
  - Light Chain ELISA
  - Immunoblotting, SDS-PAGE and Immunoprecipitation
  - [^{35}S] Metabolic Labeling
- QUANTIFICATION AND STATISTICAL ANALYSIS
  - Mass Spectrometry Interactomics TMT and SILAC Quantification
  - Statistical Analysis of Biochemical Experiment
- DATA AND SOFTWARE AVAILABILITY

SUPPLEMENTAL INFORMATION

Supplemental Information can be found online at https://doi.org/10.1016/j.chembiol.2019.04.001.

ACKNOWLEDGMENTS

We thank Evan Powers for critical reading of the manuscript. We thank NIH (DK107604, to R.L.W.) for financial support. L.P. and B.R. were both supported by Leukemia and Lymphoma Society postdoctoral fellowships. J.C.G. was supported by an American Heart Association postdoctoral fellowship.

AUTHOR CONTRIBUTIONS

R.L.W. oversaw and guided the project. J.W.K. provided additional guidance on the project. L.P., B.R., B.N., and J.C.G. designed and carried out experiments and analyzed the data. L.P., B.R., and R.L.W. prepared the figures and wrote the manuscript.

DECLARATION OF INTERESTS

The authors declare no competing interests.

Received: January 29, 2019
Revised: March 14, 2019
Accepted: March 31, 2019
Published: May 16, 2019

REFERENCES

Adachi, Y., Yamamoto, K., Okada, T., Yoshida, H., Harada, A., and Mori, K. (2008). ATF6 is a transcription factor specializing in the regulation of quality control proteins in the endoplasmic reticulum. Cell Struct. Funct. *33*, 75–89.

Arendt, B.K., Ramirez-Alvarado, M., Sikkink, L.A., Keats, J.J., Ahmann, G.J., Dispenzieri, A., Fonseca, R., Ketterling, R.P., Knudson, R.A., Mulvihill, E.M., et al. (2008). Biologic and genetic characterization of the novel amyloidogenic lambda light chain-secreting human cell lines, ALMC-1 and ALMC-2. Blood *112*, 1931–1941.

Balchin, D., Hayer-Hartl, M., and Hartl, F.U. (2016). In vivo aspects of protein folding and quality control. Science *353*, aac4354.

Behnke, J., Feige, M.J., and Hendershot, L.M. (2015). BiP and its nucleotide exchange factors Grp170 and Sil1: mechanisms of action and biological functions. J. Mol. Biol. *427*, 1589–1608.

Behnke, J., Mann, M.J., Scruggs, F.L., Feige, M.J., and Hendershot, L.M. (2016). Members of the Hsp70 family recognize distinct types of sequences to execute er quality control. Mol. Cell *63*, 739–752.

Blancas-Mejia, L.M., and Ramirez-Alvarado, M. (2013). Systemic amyloidoses. Annu. Rev. Biochem. *82*, 745–774.

Braakman, I., and Bulleid, N.J. (2011). Protein folding and modification in the mammalian endoplasmic reticulum. Annu. Rev. Biochem. *80*, 71–99.

Budayeva, H.G., and Cristea, I.M. (2014). A mass spectrometry view of stable and transient protein interactions. Adv. Exp. Med. Biol. *806*, 263–282.

Chen, J.J., Genereux, J.C., Qu, S., Hulleman, J.D., Shoulders, M.D., and Wiseman, R.L. (2014). ATF6 activation reduces the secretion and extracellular aggregation of destabilized variants of an amyloidogenic protein. Chem. Biol. *21*, 1564–1574.

Chiang, W.C., Hiramatsu, N., Messah, C., Kroeger, H., and Lin, J.H. (2012). Selective activation of ATF6 and PERK endoplasmic reticulum stress signaling pathways prevent mutant rhodopsin accumulation. Invest. Ophthalmol. Vis. Sci. *53*, 7159–7166.

Christianson, J.C., Olzmann, J.A., Shaler, T.A., Sowa, M.E., Bennett, E.J., Richter, C.M., Tyler, R.E., Greenblatt, E.J., Harper, J.W., and Kopito, R.R. (2011). Defining human ERAD networks through an integrative mapping strategy. Nat. Cell Biol. *14*, 93–105.

Cole, K.S., Grandjean, J.M.D., Chen, K., Witt, C.H., O'Day, J., Shoulders, M.D., Wiseman, R.L., and Weerapana, E. (2018). Characterization of an A-site selective protein disulfide isomerase A1 inhibitor. Biochemistry *57*, 2035–2043.

Cooley, C.B., Ryno, L.M., Plate, L., Morgan, G.J., Hulleman, J.D., Kelly, J.W., and Wiseman, R.L. (2014). Unfolded protein response activation reduces secretion and extracellular aggregation of amyloidogenic immunoglobulin light chain. Proc. Natl. Acad. Sci. U S A *111*, 13046–13051.

Davis, D.P., Khurana, R., Meredith, S., Stevens, F.J., and Argon, Y. (1999). Mapping the major interaction between binding protein and Ig light chains to sites within the variable domain. J. Immunol. *163*, 3842–3850.

Feige, M.J., and Buchner, J. (2014). Principles and engineering of antibody folding and assembly. Biochim. Biophys. Acta *1844*, 2024–2031.

Fonslow, B.R., Niessen, S.M., Singh, M., Wong, C.C., Xu, T., Carvalho, P.C., Choi, J., Park, S.K., and Yates, J.R., 3rd (2012). Single-step inline hydroxyapatite enrichment facilitates identification and quantitation of phosphopeptides from mass-limited proteomes with MudPIT. J. Proteome Res. *11*, 2697–2709.

Genereux, J.C., Qu, S., Zhou, M., Ryno, L.M., Wang, S., Shoulders, M.D., Kaufman, R.J., Lasmezas, C.I., Kelly, J.W., and Wiseman, R.L. (2015). Unfolded protein response-induced ERdj3 secretion links ER stress to extracellular proteostasis. EMBO J. *34*, 4–19.

Guerriero, C.J., and Brodsky, J.L. (2012). The delicate balance between secreted protein folding and endoplasmic reticulum-associated degradation in human physiology. Physiol. Rev. *92*, 537–576.

He, L., Diedrich, J., Chu, Y.-Y., and Yates, J.R. (2015). Extracting accurate precursor information for tandem mass spectra by rawconverter. Anal. Chem. *87*, 11361–11367.

Hellman, R., Vanhove, M., Lejeune, A., Stevens, F.J., and Hendershot, L.M. (1999). The in vivo association of BiP with newly synthesized proteins is dependent on the rate and stability of folding and not simply on the presence of sequences that can bind to BiP. J. Cell Biol. *144*, 21–30.

Hetz, C., and Saxena, S. (2017). ER stress and the unfolded protein response in neurodegeneration. Nat. Rev. Neurol. *13*, 477–491.

Hosp, F., Vossfeldt, H., Heinig, M., Vasiljevic, D., Arumughan, A., Wyler, E., Landthaler, M., Hubner, N., Wanker, E.E., Lannfelt, L., et al. (2015). Quantitative interaction proteomics of neurodegenerative disease proteins. Cell Rep. *11*, 1134–1146.

Hsu, T.A., Watson, S., Eiden, J.J., and Betenbaugh, M.J. (1996). Rescue of immunoglobulins from insolubility is facilitated by PDI in the baculovirus expression system. Protein Expr. Purif. *7*, 281–288.

Huttlin, E.L., Ting, L., Bruckner, R.J., Gebreab, F., Gygi, M.P., Szpyt, J., Tam, S., Zarraga, G., Colby, G., Baltier, K., et al. (2015). The bioplex network: a systematic exploration of the human interactome. Cell *162*, 425–440.

Katrina Meyer, M.S. (2015). Quantitative affinity purification mass spectrometry: a versatile technology to study protein-protein interactions. Front. Genet. *6*, 237.

Kean, M.J., Couzens, A.L., and Gingras, A.C. (2012). Mass spectrometry approaches to study mammalian kinase and phosphatase associated proteins. Methods *57*, 400–408.

Kim, Y.E., Hipp, M.S., Bracher, A., Hayer-Hartl, M., and Hartl, F.U. (2013). Molecular chaperone functions in protein folding and proteostasis. Annu. Rev. Biochem. *82*, 323–355.

Lee, A.H., Iwakoshi, N.N., and Glimcher, L.H. (2003). XBP-1 regulates a subset of endoplasmic reticulum resident chaperone genes in the unfolded protein response. Mol. Cell. Biol. *23*, 7448–7459.

Lomant, A.J., and Fairbanks, G. (1976). Chemical probes of extended biological structures: synthesis and properties of the cleavable protein cross-linking reagent [^{35}S]dithiobis(succinimidyl propionate). J. Mol. Biol. *104*, 243–261.

McAlister, G.C., Huttlin, E.L., Haas, W., Ting, L., Jedrychowski, M.P., Rogers, J.C., Kuhn, K., Pike, I., Grothe, R.A., Blethrow, J.D., et al. (2012). Increasing the multiplexing capacity of TMTs using reporter ion isotopologues with isobaric masses. Anal. Chem. *84*, 7469–7478.

McAlister, G.C., Nusinow, D.P., Jedrychowski, M.P., Wühr, M., Huttlin, E.L., Erickson, B.K., Rad, R., Haas, W., and Gygi, S.P. (2014). MultiNotch MS3 enables accurate, sensitive, and multiplexed detection of differential expression across cancer cell line proteomes. Anal. Chem. *86*, 7150–7158.

Melnick, J., Aviel, S., and Argon, Y. (1992). The endoplasmic reticulum stress protein GRP94, in addition to BiP, associates with unassembled immunoglobulin chains. J. Biol. Chem. *267*, 21303–21306.

Melnick, J., Dul, J.L., and Argon, Y. (1994). Sequential interaction of the chaperones BiP and GRP94 with immunoglobulin chains in the endoplasmic reticulum. Nature *370*, 373–375.

Miteva, Y.V., Budayeva, H.G., and Cristea, I.M. (2013). Proteomics-based methods for discovery, quantification, and validation of protein-protein interactions. Anal. Chem. *85*, 749–768.

Morgan, G.J., and Kelly, J.W. (2016). The kinetic stability of a full-length antibody light chain dimer determines whether endoproteolysis can release amyloidogenic variable domains. J. Mol. Biol. *428*, 4280–4297.

Nittis, T., Guittat, L., LeDuc, R.D., Dao, B., Duxin, J.P., Rohrs, H., Townsend, R.R., and Stewart, S.A. (2010). Revealing novel telomere proteins using in vivo cross-linking, tandem affinity purification, and label-free quantitative LC-FTICR-MS. Mol. Cell. Proteomics *9*, 1144–1156.

Ong, S.-E., Blagoev, B., Kratchmarova, I., Kristensen, D.B., Steen, H., Pandey, A., and Mann, M. (2002). Stable isotope labeling by amino acids in cell culture, SILAC, as a simple and accurate approach to expression proteomics. Mol. Cell. Proteomics *1*, 376–386.

Ow, S.Y., Salim, M., Noirel, J., Evans, C., and Wright, P.C. (2011). Minimising iTRAQ ratio compression through understanding LC-MS elution dependence and high-resolution HILIC fractionation. Proteomics *11*, 2341–2346.

Pankow, S., Bamberger, C., Calzolari, D., Bamberger, A., and Yates, J.R., 3rd (2016). Deep interactome profiling of membrane proteins by co-interacting protein identification technology. Nat. Protoc. *11*, 2515–2528.

Pankow, S., Bamberger, C., Calzolari, D., Martinez-Bartolome, S., Lavallee-Adam, M., Balch, W.E., and Yates, J.R., 3rd (2015). F508 CFTR interactome remodelling promotes rescue of cystic fibrosis. Nature *528*, 510–516.

Papachristou, E.K., Kishore, K., Holding, A.N., Harvey, K., Roumeliotis, T.I., Chilamakuri, C.S.R., Omarjee, S., Chia, K.M., Swarbrick, A., Lim, E., et al. (2018). A quantitative mass spectrometry-based approach to monitor the dynamics of endogenous chromatin-associated protein complexes. Nat. Commun. *9*, 986.

Park, S.K.R., Aslanian, A., McClatchy, D.B., Han, X., Shah, H., Singh, M., Rauniyar, N., Moresco, J.J., Pinto, A.F.M., Diedrich, J.K., et al. (2014). Census 2: isobaric labeling data analysis. Bioinformatics *30*, 2208–2209.

Petrova, K., Oyadomari, S., Hendershot, L.M., and Ron, D. (2008). Regulated association of misfolded endoplasmic reticulum lumenal proteins with P58/DNAJc3. EMBO J. *27*, 2862–2872.

Plate, L., Cooley, C.B., Chen, J.J., Paxman, R.J., Gallagher, C.M., Madoux, F., Genereux, J.C., Dobbs, W., Garza, D., Spicer, T.P., et al. (2016). Small molecule proteostasis regulators that reprogram the ER to reduce extracellular protein aggregation. eLife *5*, https://doi.org/10.7554/eLife.15550.

Plate, L., and Wiseman, R.L. (2017). Regulating secretory proteostasis through the unfolded protein response: from function to therapy. Trends Cell Biol. *27*, 722–737.

Powers, E.T., Morimoto, R.I., Dillin, A., Kelly, J.W., and Balch, W.E. (2009). Biological and chemical approaches to diseases of proteostasis deficiency. Annu. Rev. Biochem. *78*, 959–991.

Roumeliotis, T.I., Williams, S.P., Gonçalves, E., Alsinet, C., Del Castillo Velasco-Herrera, M., Aben, N., Ghavidel, F.Z., Michaut, M., Schubert, M., Price, S., et al. (2017). Genomic determinants of protein abundance variation in colorectal cancer cells. Cell Rep. *29*, 2201–2214.

Rutkowski, D.T., Kang, S.W., Goodman, A.G., Garrison, J.L., Taunton, J., Katze, M.G., Kaufman, R.J., and Hegde, R.S. (2007). The role of p58IPK in protecting the stressed endoplasmic reticulum. Mol. Biol. Cell *18*, 3681–3691.

Savitski, M.M., Mathieson, T., Zinn, N., Sweetman, G., Doce, C., Becher, I., Pachl, F., Kuster, B., and Bantscheff, M. (2013). Measuring and managing ratio compression for accurate iTRAQ/TMT quantification. J. Proteome Res. *12*, 3586–3598.

Shen, Y., and Hendershot, L.M. (2005). ERdj3, a stress-inducible endoplasmic reticulum DnaJ homologue, serves as a cofactor for BiP's interactions with unfolded substrates. Mol. Biol. Cell *16*, 40–50.

Shoulders, M.D., Ryno, L.M., Genereux, J.C., Moresco, J.J., Tu, P.G., Wu, C., Yates, J.R., 3rd, Su, A.I., Kelly, J.W., and Wiseman, R.L. (2013). Stress-independent activation of XBP1s and/or ATF6 reveals three functionally diverse ER proteostasis environments. Cell Rep. *3*, 1279–1292.

Skowronek, M.H., Hendershot, L.M., and Haas, I.G. (1998). The variable domain of nonassembled Ig light chains determines both their half-life and binding to the chaperone BiP. Proc. Natl. Acad. Sci. U S A *95*, 1574–1578.

Smith, A.L., Friedman, D.B., Yu, H., Carnahan, R.H., and Reynolds, A.B. (2011a). ReCLIP (reversible cross-link immuno-precipitation): an efficient method for interrogation of labile protein complexes. PLoS One *6*, e16206.

Smith, S.E., Granell, S., Salcedo-Sicilia, L., Baldini, G., Egea, G., Teckman, J.H., and Baldini, G. (2011b). Activating transcription factor 6 limits intracellular accumulation of mutant alpha(1)-antitrypsin Z and mitochondrial damage in hepatoma cells. J. Biol. Chem. *286*, 41563–41577.

Storey, J.D., and Tibshirani, R. (2003). Statistical significance for genomewide studies. Proc. Natl. Acad. Sci. U S A *100*, 9440–9445.

Tabb, D.L., McDonald, W.H., and Yates, J.R. (2002). DTASelect and contrast: tools for assembling and comparing protein identifications from shotgun proteomics. J. Proteome Res. *1*, 21–26.

Taipale, M., Tucker, G., Peng, J., Krykbaeva, I., Lin, Z.Y., Larsen, B., Choi, H., Berger, B., Gingras, A.C., and Lindquist, S. (2014). A quantitative chaperone interaction network reveals the architecture of cellular protein homeostasis pathways. Cell *158*, 434–448.

Ting, L., Rad, R., Gygi, S.P., and Haas, W. (2011). MS3 eliminates ratio distortion in isobaric multiplexed quantitative proteomics. Nat. Methods *8*, 937–940.

Wall, J., Schell, M., Murphy, C., Hrncic, R., Stevens, F.J., and Solomon, A. (1999). Thermodynamic instability of human lambda 6 light chains: correlation with fibrillogenicity. Biochemistry *38*, 14101–14108.

Washburn, M.P., Wolters, D., and Yates, J.R., 3rd (2001). Large-scale analysis of the yeast proteome by multidimensional protein identification technology. Nat. Biotechnol. *19*, 242–247.

Wiseman, R.L., Powers, E.T., Buxbaum, J.N., Kelly, J.W., and Balch, W.E. (2007). An adaptable standard for protein export from the endoplasmic reticulum. Cell *131*, 809–821.

Xu, T., Park, S.K., Venable, J.D., Wohlschlegel, J.A., Diedrich, J.K., Cociorva, D., Lu, B., Liao, L., Hewel, J., Han, X., et al. (2015). ProLuCID: an improved SEQUEST-like algorithm with enhanced sensitivity and specificity. J. Proteomics *3*, 16–24.

Yamamoto, K., Yoshida, H., Kokame, K., Kaufman, R.J., and Mori, K. (2004). Differential contributions of ATF6 and XBP1 to the activation of endoplasmic reticulum stress-responsive cis-acting elements ERSE, UPRE and ERSE-II. J. Biochem. *136*, 343–350.

Yates, J.R., Ruse, C.I., and Nakorchevsky, A. (2009). Proteomics by mass spectrometry: approaches, advances, and applications. Annu. Rev. Biomed. Eng. *11*, 49–79.

STAR★METHODS

KEY RESOURCES TABLE

REAGENT or RESOURCE	SOURCE	IDENTIFIER
Antibodies		
KDEL (mouse monoclonal 10C3)	Enzo Life Sciences	Cat#ADI-SPA-827-D
M2 anti-FLAG (mouse monoclonal)	Sigma Aldrich	Cat#F3165
Anti-α-Tubulin (mouse monoclonal B-5-1-2)	Sigma Aldrich	Cat#T5168
BiP/GRP-78 (mouse monoclonal E-4)	Santa Cruz Biotechnology	Cat#sc-166490,
β-actin (mouse monoclonal AC-15)	Sigma Aldrich	Cat#A1978
GRP94 (rabbit polyclonal N1N3)	GenTex	Cat#GTX103203
HYOU1 (ORP150) (rabbit polyclonal C2C3)	GenTex	Cat#GTX102255
ERdj3 (DNAJB11) (rabbit polyclonal)	ProteinTech	Cat#15484-1-AP
PDIA4 (ERp72) (rabbit polyclonal)	ProteinTech	Cat#14712-1-AP
PDIA6 (rabbit polyclonal N1N3)	GenTex	Cat#GTX121275
PDIA3 (ERp57) (rabbit polyclonal G117)	CellSignaling	Cat#2881S
free λ LC antibody (sheep polyclonal)	Bethyl Laboratories	Cat#P80-127
HRP-conjugated goat anti-human λ light chain antibody	Bethyl Laboratories	Cat#A80-116P
Chemicals, Peptides, and Recombinant Proteins		
^{13}C6,^{15}N4-*L*-Arginine	Cambridge Isotopes Laboratories	Cat#CNLM-539-H
Anti-FLAG M1 agarose affinity gel	Sigma Aldrich	Cat#A4596-5ML
Tris(2-carboxyethyl)phosphine hydrochloride (TCEP-HCl)	ThermoFisher	Cat#20490
Trypsin (Sequencing grade modified)	Promega	Cat#5111
Iodoacetamide	Sigma Aldrich	Cat#I6125
RapiGest SF Surfactant	Waters	Cat#186001861
purified human Bence Jones λ light chain	Bethyl Laboratories	Cat#P80-127
EasyTag EXPRESS [35S] Protein Labeling Mix	PerkinElmer	Cat#NEG772002MC
Critical Commercial Assays		
SILAC Protein Quantification kit – DMEM	ThermoFisher	Cat#A33969
TMTsixplex Isobaric Label Reagent Set	ThermoFisher	Cat#90066
Experimental Models: Cell Lines		
HEK293^{DAX} cells	this group, Shoulders et al., 2013	HEK293^{DAX}
Recombinant DNA		
Mammalian expression plasmid (pCMV1) for ^{FT}ALLC	this group, Cooley et al., 2014	ss.FT.ALLC-pCMV1
Mammalian expression plasmid (pCMV1) for ^{FT}JTO	this group, Cooley et al., 2014	ss.FT.JTO-pCMV1
Mammalian expression plasmid (pDEST40) for untagged ALLC	this group, Cooley et al., 2014	ss.ALLC-pDEST40
Entry plasmid (gateway cloning) for GRP94, GRP94.pDONR223	Addgene	Cat #82130
Mammalian expression plasmid (pDEST40) for GRP94	this paper, Genereux et al., 2015	GRP94.pDEST40
Mammalian expression plasmid for ^{FT}BiP	this group, Genereux et al., 2015	pFLAG.BiP.WT
Mammalian expression plasmid (pDEST40) for ERdj3	this group, Genereux et al., 2015	ss.ERdj3.pDEST40
Software and Algorithms		
Integrated Proteomics Pipeline Suite (IP2)	Integrated Proteomics Applications, Inc.	N/A
RawConverter	He et al., 2015	N/A
ProLuCID (IP2 Suite)	Xu et al., 2015	N/A
DTASelect (IP2 Suite)	Tabb et al., 2002	N/A
Census (IP2 Suite)	Park et al., 2014	N/A

CONTACT FOR REAGENT AND RESOURCE SHARING

Further information and requests for resources and reagents should be directed to and will be fulfilled by the Lead Contact, R. Luke Wiseman (wiseman@scripps.edu).

EXPERIMENTAL MODEL AND SUBJECT DETAILS

Cell Culture and Transfections

The creation and maintenance of HEK293^{DAX} cells has been described previously (Shoulders et al., 2013). Briefly, HEK293^{DAX} cells were cultured in high-glucose Dulbecco's Modified Eagle's Medium (DMEM; Corning-Cellgro) supplemented with 10% fetal bovine serum (FBS; Omega Scientific), 2 mM L-glutamine (Gibco), 100 U*mL^{-1} penicillin, and 100 μg*mL^{-1} streptomycin (Gibco). All cells were cultured under typical tissue culture conditions (37°C, 5% CO_2). Cells were routinely tested for mycoplasma every 6 months. No further authentication of cell lines was performed by the authors. Cells were transfected using calcium phosphate precipitation, as previously described (Shoulders et al., 2013). All plasmids for transfection were prepared using the Qiagen Midiprep kit according to the manufacturers protocol. For SILAC experiments, the SILAC Protein Quantification kit – DMEM (ThermoFisher) was purchased. In addition to the supplied $^{13}C_6$-*L*-Lys, the heavy media was also supplemented with $^{13}C_6$,$^{15}N_4$-*L*-Arg (Cambridge Isotopes Laboratories, Inc.). Light- and heavy-labeled HEK293^{DAX} cells were generated for a previously study (Shoulders et al., 2013). Cells were cultured additionally for a minimum of 5 passages in heavy SILAC DMEM media prior to transfection to ensure full heavy-isotope incorporation.

METHOD DETAILS

Plasmids and Antibodies

Plasmids expressing ^{FT}ALLC, ^{FT}JTO, or untagged ALLC in the pCMV1 or pDEST40 vector were described previously (Cooley et al., 2014). ^{FT}BiP and ERdj3 overexpression plasmids were used as described previously (Genereux et al., 2015). The GRP94 overexpression plasmid was prepared using GRP94.pDONR223 (Addgene; Cat #82130), which was recombined into pDEST40 using Gateway cloning according to the manufacturers protocol. Primary antibodies were acquired from commercial sources and used at the indicated dilutions in Antibody Buffer (50 mM Tris [pH 7.5], 150 mM NaCl supplemented with 5% BSA and 0.1% NaN_3). Mouse monoclonal antibodies were used to detect KDEL (1:1000, Enzo Life Sciences), M2 anti-FLAG (1:500, Sigma Aldrich), Tubulin [B-5-1-2] (1:4000,Sigma), BiP/GRP-28 (1:500, Santa Cruz Biotechnology), β-actin (1:10000, Sigma Aldrich). Polyclonal rabbit antibodies were used to detect GRP94 (1:1000, GeneTex), HYOU1 (1:1000, GeneTex), ERdj3 (DNAJB11) (1:1000, ProteinTech), PDIA4 (1:1000, ProteinTech), PDIA6 (1:1000, GenTex), PDIA3 (ERp57) (1:1000, CellSignaling).

Affinity-Purification of LC Samples and MS Sample Preparation

In general, a 10 cm tissue culture plate of HEK293^{DAX} cells was transfected with the appropriate LC expression plasmids and a fully confluent plate (approximately 10^7 cells) was used per condition. Cell harvest, cross-linking, lysis and co-immunoprecipitation were carried out as described in the Supplemental Information. Proteins were eluted from anti-M1 FLAG agarose beads (Sigma) twice in 75μL elution buffer (10mM Tris [pH 7.5], 2% SDS, 1mM EDTA) by heating to 95°C for 5 min. Eluted fractions were combined and proteins were precipitated in methanol/chloroform, washed twice in methanol, and then air dried. For SILAC experiments, protein pellets were resuspended in 50μL 8M urea, 50mM Tris pH 8.0, reduced with 10mM TCEP (ThermoFisher) for 30 min at room temperature, and alkylated with 12 mM iodoacetamide (Sigma) for 30min in the dark. Samples were then diluted four-fold in 50mM Tris to lower the urea concentration. For TMT experiments, the protein pellets were resuspended in 3 – 5μL 1% RapiGest SF Surfactant (Waters) followed by addition of HEPES buffer (pH 8.0, 50 mM) to a volume of 50μL. Samples were reduced with 5mM TCEP for 30min at room temperature and alkylated with 10mM iodoacetamide for 30min in the dark. Trypsin (0.5μg, Sequencing grade, Promega) was then added to the SILAC or TMT samples and incubated for 16 hours at 37°C while shaking. After digestion, SILAC peptides samples were acidified with formic acid (5% final concentration) and directly proceeded to LC-MS analysis. TMT samples were first reacted with NHS-modified TMT sixplex reagents (ThermoFisher) in 40% v/v acetonitrile and incubated for 60 min at room temperature. Reactions were then quenched by addition of 0.4% (w/v) ammonium bicarbonate. The digested and labeled samples for a given sixplex experiment were pooled and acidified with formic acid (5% final concentration). Samples were concentrated on a SpeedVac and rediluted in buffer A (94.9% water, 5% acetonitrile, 0.1 formic acid, v/v/v). Cleaved Rapigest SF and debris was removed by centrifugation for 30min at 18,000x g.

Mass Spectrometry and Interactome Characterization

MuDPIT microcolumns were prepared as described (Fonslow et al., 2012), peptide samples were directly loaded onto the columns using a high-pressure chamber (Shotgun Proteomics Inc), and the columns were washed for 30min with buffer A. LC-MS/MS analysis was performed using a Q-Exactive mass spectrometer equipped with an EASY nLC 1000 (Thermo Fisher). MuDPIT experiments were performed by 10 μL sequential injections of 0, 20, 50, 80, 100% buffer C (500 mM ammonium acetate in buffer A) and a final step of 90% buffer C / 10% buffer B (19.9% water, 80% acetonitrile, 0.1% formic acid, v/v/v) and each step followed by a gradient from buffer A to buffer B on a 18 cm fused silica microcapillary column (ID 100μm) ending in a laser-pulled tip filled with Aqua C18,

3μm, 100Å resin (Phenomenex). Electrospray ionization (ESI) was performed directly from the analytical column by applying a voltage of 2.5 kV with an inlet capillary temperature of 275°C. Data-dependent acquisition of MS/MS spectra was performed with the following settings: eluted peptides were scanned from 400 to 1800 m/z with a resolution of 70,000 and the mass spectrometer in a data dependent acquisition mode. The top ten peaks for each full scan were fragmented by HCD using normalized collision energy of 30%, 2.0 m/z isolation window, 120 ms max integration time, a resolution of 7500, scanned from 100 to 1800 m/z, and dynamic exclusion set to 60s. Peptide identification and SILAC- or TMT-based protein quantification was performed using the Integrated Proteomics Pipeline Suite IP2 (Integrated Proteomics Applications, Inc.) and modules ProLuCID, DTASelect and Census (Park et al., 2014; Tabb et al., 2002; Xu et al., 2015). MS2 spectra were extracted from Thermo XCalibur .raw file format using RawConverter (He et al., 2015). Spectra were searched using ProLuCID against a Uniprot human proteome database (release date 05/2014). The database was curated to remove redundant protein and splice-isoforms, and the sequences for the variable domains of ^{FT}ALLC and ^{FT}JTO and the shared constant domain were added. Searches were carried out using a decoy database of reversed peptide sequences and the following search parameters: 50 ppm peptide precursor tolerance, 0.6 Da fragment mass tolerance, 6 amino acid minimum peptide length, trypsin cleavage (max. 2 missed cleavage events), static Cys modification of 57.0215 (carbamidomethylation), and static N-terminal and Lys modification of 229.1629 (TMT-sixplex). ProLuCID search results were filtered using DTASelect using combined XCorr and DeltaCN scores to minimize the peptide false discovery rate at 1% and minimum of 2 peptides per protein ID. TMT reporter ion intensities were extracted in Census using a mass tolerance of 0.05 Da and summed for individual peptides belonging to the same protein. SILAC data was processed similarly, except static modification from the TMT-sixplex were omitted, and heavy [^{15}N, ^{13}C]-Lys and Arg modifications were included in the ProLuCID search.

Light Chain ELISA

Transfected HEK293^{DAX} were plated 150,000 cells/well in 2 identical 48-well plates (Genessee Scientific) containing 500 μL of media. Media was removed and wells were washed two times with 250 μL media containing 50 μg/mL cycloheximide (CHX). One plate was washed two times with 1x PBS and cell lysates prepared in RIPA buffer. This sample was used to monitor lysate levels of LC at t=0 h. The second plate was incubated 250 μL media with CHX for 4 h and conditioned media was collected. This sample was used to monitor secreted LC levels at 4 h. Free LC concentrations were determined by ELISA in 96-well plates (Immulon 4HBX, Thermo Fisher), as previously described (Cooley et al., 2014; Plate et al., 2016). Briefly, wells were coated overnight at 37°C with sheep polyclonal free λ LC antibody (Bethyl Laboratories, A80-127A) at a 1:500 dilution in 50 mM sodium carbonate (pH 9.6). In between all incubation steps, the plates were rinsed extensively with Tris-buffered saline containing 0.05% Tween-20 (TBST). Plates were blocked with 5% non-fat dry milk in TBST for 1 hr at 37°C. Media analytes were diluted between 5 – 200-fold in 5% non-fat dry milk in TBST and 100 μL of each sample was added to individual wells. Light chain standards ranging from 3 – 300 ng/mL were prepared from purified human Bence Jones λ light chain (Bethyl Laboratories, P80-127). Plates were incubated at 37°C for 1.5 h with shaking. Finally, HRP-conjugated goat anti-human λ light chain antibody (Bethyl Laboratories, A80-116P) was added at a 1: 5,000 dilution in 5% non-fat dry milk in TBST, followed by a 1.5 h incubation of the plates at 37°C. The detection was carried out with 2,2'-azinobis(3-ethylbenzothiazoline-6-sulfonic acid) (ABTS, 0.18 mg/mL) and 0.03% hydrogen peroxide in 100 mM sodium citrate pH 4.0. Detection solution (100 μL) was added to each well and the plates were incubated at room temperature. The absorbance was recorded at 405 nm and the values for the LC standards were fitted to a 4-parameter logistic function. LC concentrations were averaged from at least 3 independent replicates under each treatment and then normalized to vehicle conditions. Fraction secreted was then calculated using the equation: fraction secreted = [LC] in media at t=4 h / [LC] lysate at t = 0 h.

Immunoblotting, SDS-PAGE and Immunoprecipitation

Cell lysates were prepared as previously described in RIPA buffer (50 mM Tris, pH 7.5, 150 mM NaCl, 0.1 % SDS, 1% Triton X-100, 0.5% deoxycholate and protease inhibitor cocktail (Roche). Total protein concentration in cellular lysates was normalized using the Bio-Rad protein assay. Lysates were then denatured with 1X Laemmli buffer + 100 mM DTT and boiled before being separated by SDS-PAGE. Samples were transferred onto nitrocellulose membranes (Bio-Rad) for immunoblotting and blocked with 5% milk in Tris-buffered saline, 0.5 % Tween-20 (TBST) following incubation overnight at 4°C with primary antibodies. Membranes were washed in TBST, incubated with IR-Dye conjugated secondary antibodies and analyzed using Odyssey Infrared Imaging System (LI-COR Biosciences). Quantification was carried out with LI-COR Image Studio software. For immunoprecipitations, cells were washed with PBS and then treated with the indicated concentration Dithiobis(succinimidiyl propionate) (DSP) for 30 min at room temperature. The crosslinking reaction was quenched by addition of 100 mM Tris pH 7.5 for 15 min, then lysates were prepared in RIPA buffer. Total protein concentration in cellular lysates was normalized using Bio-Rad protein assay. Cell lysates were then subjected to preclearing with Sepharose 4B beads (Sigma) at 4°C for 1 h with agitation. The precleared lysates were then subjected to immunoprecipitation with a M1 anti-Flag agarose resin (Sigma) at 4°C overnight. After four washes in RIPA buffer, proteins were eluted by boiling in 6x Laemmli buffer and 100 mM DTT. Blots from IPs and inputs were probed with the primary antibodies. Membranes were then treated as described above.

[^{35}S] Metabolic Labeling

[^{35}S] metabolic labeling experiments were performed as previously described (Cooley et al., 2014; Shoulders et al., 2013). Briefly, transfected HEK293^{DAX} were plated on poly-D-lysine coated 6-well plates and metabolically labeled in DMEM-Cys/-Met (Corning CellGro, Mediatech Inc., Manassas, VA) supplemented with glutamine, penicillin/streptomycin, dialyzed fetal bovine serum, and

EasyTag EXPRESS [^{35}S] Protein Labeling Mix (Perkin Elmer) for 30 min. Cells were washed twice with complete media and incubated in pre-warmed DMEM for the indicated times. Media or lysates were harvested at the indicated times. Lysates were prepared in RIPA buffer (50mM Tris [pH 7.5], 150mM NaCl, 1% Triton X100, 0.5% sodium deoxycholate, 0.1% SDS) containing proteases inhibitors cocktail (Roche). FLAG-tagged LC variants were immunopurified using M1 anti-FLAG agarose beads (Sigma Aldrich) and washed four times with RIPA buffer. The immunoisolates were then eluted by boiling in 6X Laemmli buffer and separated on 12% SDS-PAGE. Gels were stained with Coomassie Blue, dried, exposed to phosphorimager plates (GE Healthcare, Pittsburgh, PA) and imaged by autoradiography using a Typhoon Trio Imager (GE Healthcare). Band intensities were quantified by densitometry in ImageQuant. Fraction secreted was calculated using the equation: fraction secreted = [extracellular [^{35}S]-LC signal at t / (extracellular [^{35}S]-LC signal at t=0 + intracellular [^{35}S]-LC signal at t=0)]. Fraction remaining was calculated using the equation: [(extracellular [^{35}S]-LC signal at t + intracellular [^{35}S]-LC signal at t) / (extracellular [^{35}S]-LC signal at t=0 + intracellular [^{35}S]-LC signal at t=0)].

QUANTIFICATION AND STATISTICAL ANALYSIS

Mass Spectrometry Interactomics TMT and SILAC Quantification

Quantification of heavy and light peptide intensities was carried out in Census using MS1 spectral files extracted using RawConverter. Data normalization for TMT reporter intensities and SILAC ratios was carried out manually. For SILAC experiments, the SILAC heavy/light ratios for each quantified protein were normalized to the ratio observed for ^{FT}ALLC or ^{FT}JTO. Each experiment represented a comparison of an experimental condition (light sample) against a common heavy reference sample (^{FT}ALLC, vehicle treated). Comparisons between experimental conditions were expressed as ratios of the LC-normalized SILAC ratios. For TMT experiments, the unnormalized TMT reporter ion intensities for each quantified protein were normalized against the intensities observed for ^{FT}ALLC according to the following formula:

$$I^{norm}_{n,TMT_i} = I^{un}_{n,TMT_i} \cdot \frac{\sum^{TMT_j}_{TMT_i} I^{un}_{LC}}{I^{un}_{LC,TMT_i}}, \quad \text{(Equation 1)}$$

where I^{norm}_n and I^{un}_n are the normalized and unnormalized TMT intensities, respectively, for a given protein *n* in the TMT channels *i-j*. Channels that did not contain LC (e.g. control transfections with untagged ALLC) were omitted from the normalization. For interactome comparison between ^{FT}ALLC and ^{FT}JTO, only shared peptides from the λ V_c constant domain were considered for the normalization. Interaction fold changes were expressed as $\log_2$ differences of the normalized TMT intensities for a given protein between respective TMT channels (experimental conditions), according to the following formula:

$$\log_2 I^{norm}_{n,TMT_i} - \log_2 I^{norm}_{n,TMT_j}. \quad \text{(Equation 2)}$$

The mean of the $\log_2$ interaction difference was calculated from multiple MuDPIT LC-MS runs, which each represented an individual biological replicate. Significance of interaction differences was assessed by a two-tailed unpaired student's t-test of the normalized log2-transformed TMT intensities, followed by multiple-testing correction via FDR estimation using the method of Storey et al. (Storey and Tibshirani, 2003).

Statistical Analysis of Biochemical Experiment

Data are presented as mean ± SEM and were analyzed by two-tailed Student's t test to determine significance, unless otherwise indicated.

DATA AND SOFTWARE AVAILABILITY

The datasets for the mass spectrometry interactomics experiments showing protein identifications and quantifications are included as Tables S1, S2, S3, and S4.